
Masters Theses

Student Theses and Dissertations

Fall 2007

CFD simulation of contact planarization

Shanti Vusirikala

Follow this and additional works at: https://scholarsmine.mst.edu/masters_theses



Part of the [Chemical Engineering Commons](#)

Department:

Recommended Citation

Vusirikala, Shanti, "CFD simulation of contact planarization" (2007). *Masters Theses*. 4597.
https://scholarsmine.mst.edu/masters_theses/4597

This thesis is brought to you by Scholars' Mine, a service of the Missouri S&T Library and Learning Resources. This work is protected by U. S. Copyright Law. Unauthorized use including reproduction for redistribution requires the permission of the copyright holder. For more information, please contact scholarsmine@mst.edu.

CFD SIMULATION OF CONTACT PLANARIZATION

by

SHANTI VUSIRIKALA

A THESIS

Presented to the Faculty of the Graduate School of the

UNIVERSITY OF MISSOURI-ROLLA

In Partial Fulfillment of the Requirements for the Degree

MASTER OF SCIENCE IN CHEMICAL ENGINEERING

2007

Approved by

Dr. Kimberly Henthorn, Advisor

Dr. Parthasakha Neogi

Dr. Kakkattukuzhy Isaac

© 2007

Shanti Vusirikala

All Rights Reserved

ABSTRACT

Semiconductor devices form the essential components of most electronic devices. The fabrication of circuit elements to manufacture these devices is done by a process known as photolithography, using photoresist layer deposition, optical masks, and etching. As feature sizes become smaller, higher optical precision is required, necessitating an optically flat surface on the photoresist layer. The surface of the photoresist layer can become uneven because of conformation to the topography of the layers underneath or a change in shape of the layer after evaporation of solvent. To combat this, Brewer Science, Inc. has developed a contact planarization process (CONTACT[®]) in which an optically flat surface is used to transfer its planarity to the surface of the photoresist. However, due to high pressure from the viscous photoresist fluid during the process, the optically flat surface becomes deformed. To solve this problem, a detailed simulation and analysis of the pressure distribution along the plate is needed to find the optimal conditions to reduce the deformation of the optically flat surface.

In the current work, the CFD package FLUENT was used to simulate the evaporation and planarization processes. An unsteady-state approach was used for the microscale geometry, a multiphase model was used for the evaporation process, and a dynamic mesh model was used for the plate motion. The plate motion simulations were carried out for three different velocities and viscosities and the pressure distribution along the plate was noted at different simulation times. It has been inferred from the simulations that the pressure on the plate can be reduced by increasing the plate velocity and decreasing the viscosity of the fluid.

ACKNOWLEDGMENTS

I am extremely grateful to my advisor, Dr. Kimberly Henthorn, for being a friend, a guide, and a great motivator who demonstrated a high level of confidence in me. Throughout my work, she gave me freedom to explore avenues of research while correcting my course and guiding me at all times. I thank Dr. Neogi and Dr. Isaac, my committee members, for the help and support they have provided throughout my Masters degree program. I should especially mention Anna Pillai, Navina Tungapindi, Mihir Dave, Frency Mathew, and Saurabh Pinge, my lab mates and friends at the same time, who gave me lots of encouragement and formed a great comfortable place to work. Special thanks go to FLUENT technical support personnel Nilesh Gandhi, Jayesh Mutyal, Eric Oseid, and Rajkumar M.J. I express my gratitude to Robert Brown and Jeremy McCutcheon, of Brewer Science Inc., for financial support during my program, the opportunity to work with Brewer Science, and important information on the planarization process itself.

On a personal note, I thank my friends Ravi Philip, Rana Gunaratnam, Anil Ramachandran, Anish Thottathil, Deepak Mohan, Sumesh Nair, and countless others at Rolla who became great friends to me and helped me let off steam and stay stress-free enabling me to do productive work on my research. Last, but at the top of my list, I thank my parents Mrutyunjaya Rao and Latha Vusirikala, and my sister Preeti Vusirikala, for the tremendous encouragement and support I have received throughout my life which has enabled me to face the challenges and achieve success.

TABLE OF CONTENTS

	Page
ABSTRACT	iii
ACKNOWLEDGMENTS	iv
LIST OF ILLUSTRATIONS	viii
LIST OF TABLES	x
NOMENCLATURE	xi
SECTION	
1. THE CHIP MANUFACTURING PROCESS.....	1
1.1. OBJECTIVES	1
1.2. INTRODUCTION	1
1.2.1. Wafer Preparation.	1
1.2.2. Fabrication Techniques for Patterning.	3
1.2.2.1 Photolithography.	3
1.2.2.2 Etching.	4
1.2.3. Fabrication Techniques for Layering.	6
1.2.4. Need for Planarization.....	8
1.2.5. Planarization Techniques..	10
1.2.5.1 Chemical-mechanical planarization.....	10
1.2.5.2 Etch-back planarization..	12
1.2.5.3 Contact planarization..	12
2. INTRODUCTION.....	14
2.1. INTRODUCTION TO CFD	14
2.2. NEED AND HISTORY OF CFD	14
2.3. GOVERNING EQUATIONS OF CFD	15
2.4. PROBLEM SOLVING TECHNIQUES.....	16
2.4.1. Problem Setup..	16
2.4.2. Discretization.....	16
2.4.2.1 Finite difference method.....	16
2.4.2.2 Finite volume method.	19

2.4.2.3 Finite element method.....	19
2.4.3. Solver Formulation.....	21
2.5. SOLUTION CONVERGENCE AND ITERATIONS.....	21
2.6. CFD TECHNIQUES.....	22
2.7. POST-PROCESSING.....	23
2.8. OVERVIEW OF FLUENT SOFTWARE	27
2.8.1. Introduction.	27
2.8.2. FLUENT Modeling Examples.	27
2.8.3. Program Structure.....	28
2.8.4. Modeling Capabilities..	29
2.8.5. Boundary Conditions.....	30
2.8.6. Multiphase Models.	31
2.8.7. Dynamic Mesh Motion.....	32
2.8.8. User Defined Functions.....	33
3. EXPERIMENTAL AND SIMULATION PROCEDURE.....	34
3.1. CONTACT PLANARIZATION PROCESS	34
3.2. VISCOSITY EXPERIMENTS	35
3.2.1. Apparatus For Viscosity Testing.....	36
3.2.2. Experimental Procedure.	37
3.3. CFD PROCEDURE	39
3.4. MODELING SETUP FOR EVAPORATION PROCESS	40
3.5. MODELING SETUP FOR THE PLATE MOTION	44
4. RESULTS AND DISCUSSION	49
4.1. VISCOSITY MEASUREMENT	49
4.2. EVAPORATION	53
4.3. DYNAMIC MESH MOTION	53
5. CONCLUSIONS AND FUTURE WORK.....	61
5.1. CONCLUSIONS.....	61
5.2. FUTURE WORK.....	61
APPENDICES	
A. GOVERNING EQUATIONS OF CFD.....	65

B. UDF FOR EVAPORATION AND CONTACT PLANARIZATION	70
REFERENCES	77
VITA	80

LIST OF ILLUSTRATIONS

	Page
Figure 1.1 Density Variations in a Wafer	2
Figure 1.2 Photolithographic Process	5
Figure 1.3 Degree of Etching.....	6
Figure 1.4 Topography Conformation	8
Figure 1.5 Change in Shape of the Photoresist	9
Figure 1.6 Height over Topography.....	9
Figure 1.7 Setup for CMP	11
Figure 1.8 Dishing and Erosion	12
Figure 1.9 Contact Planarization Process	13
Figure 2.1 A Grid Showing the Discretization Procedure	17
Figure 2.2 Elements on the Circumference of a Circle.....	20
Figure 2.3 Circle Indicating the Elemental Properties.....	20
Figure 2.4 Grid for Flow Past a Flat Plate	23
Figure 2.5 Grid of a Duct.....	24
Figure 2.6 Example of an XY Plot.....	25
Figure 2.7 Example of a Contour Plot	26
Figure 2.8 Example of a Vector Plot	26
Figure 2.9 Scatter Plot of y-Velocity and Density Along a Tube	27
Figure 2.10 Basic Structure of FLUENT Program	29
Figure 2.11 Different Mesh Elements.....	30
Figure 3.1 Photoresist Surface	34
Figure 3.2 Contact Planarization.....	35
Figure 3.3 Cone and Plate with the Testing Fluid	36
Figure 3.4 Vacuum Pump Setup	38
Figure 3.5 Geometry of the Computational Domain for the Evaporation Process	41
Figure 3.6 Computational Domain Mesh for the Evaporation Process	42
Figure 3.7 Adapted Region for the Secondary Phase	45
Figure 3.8 Mesh for the Plate Motion Showing the Different Boundary Types.....	46

Figure 3.9 Adapted Region for the Plate Motion.....	48
Figure 4.1 Percentage by Mass of Sample Evaporated.....	49
Figure 4.2 Power Law Plot for S1818 with 60% Solvent.....	50
Figure 4.3 Relationship Between Average Viscosity and Solvent Percentage of S1818.	52
Figure 4.4 Phases - S1818 and Air - Evaporation.....	53
Figure 4.5 Phases - S1818 and Air - Planarization	54
Figure 4.6 Static Pressure from 0 s to 8.00e-6 s for a Plate Velocity of 0.01 m/s	55
Figure 4.7 Static Pressure from 1.00e-5 s to 1.50e-5 s for a Plate Velocity of 0.01 m/s..	55
Figure 4.8 Comparison of Pressure and Contour Plots at a Plate Velocity of 0.01 m/s ...	56
Figure 4.9 Maximum Pressure on the Plate at a Given Time for Different Plate Velocities and a Viscosity of 22 Pa·s.....	57
Figure 4.10 Maximum Pressure on the Plate at Different Velocities of the Plate	58
Figure 4.11 Maximum Pressure on the Plate at a Given Time for Different Viscosities and a Plate Velocity of 0.01 m/s.....	59
Figure 4.12 Maximum Pressure on the Plate at Different Viscosities at a Plate Velocity of 0.01 m/s	60
Figure 5.1 Wall and Interface Locations.....	63

LIST OF TABLES

	Page
Table 3-1: Model Properties of the Evaporation Simulation	43
Table 3-2: Model Properties of the Plate Motion Simulation.....	47
Table 4-1: Flow Index Values for Different Runs of the Original Sample	51
Table 4-2: Flow Index Values for S1818 with Different Solvent Percentages.....	52

NOMENCLATURE

Symbol	Description
D	Depth of Focus [μm]
DOP	Degree of Planarization [unitless]
E	Energy [J]
\vec{F}	Force Vector [unitless]
\vec{g}	Gravity Vector [unitless]
k	Thermal Conductivity [$\text{W}/\text{m}\cdot\text{K}$]
l_i	Length of i^{th} Element [m]
m_{pq}	Mass Transfer Rate from p^{th} Phase to q^{th} Phase [kg/s]
NA	Numerical Aperture [unitless]
R	Radius of the Circle [m]
S	Source Term [$\text{kg}/\text{m}^3\cdot\text{s}$ – mass, $\text{kg}/\text{m}^2\cdot\text{s}^2$ – momentum]
t	Time [s]
T	Temperature [K]
T_h	Height of the Layer Over the Topography After Planarization [μm]
T_p	Height of the Layer Over the Topography Before Planarization [μm]
$u_{i,j}$	Velocity in the x Direction at the Point (i, j) [m/s]
\vec{v}	Velocity Vector [unitless]
v_x	Velocity in the x Direction [m/s]
v_y	Velocity in the y Direction [m/s]
W	Resolution of the Image [dpi]
α_q	Volume Fraction of q^{th} Phase [unitless]
Δx	Distance Between Successive Nodes in the x Direction [m]
Δy	Distance Between Successive Nodes in the y Direction [m]
θ	Angle Subtended at the Center of the Circle by a Sector [degrees]
λ	Wavelength [nm]

ρ_q	Density of q^{th} Phase [kg/m ³]
ϕ	Scalar Quantity [unitless]
ψ	Stream Function [m ³ /s]
∇T	Temperature Gradient [unitless]

1. THE CHIP MANUFACTURING PROCESS

1.1. OBJECTIVES

The primary objective of this project is to study pressure variations on the surface of optically flat plates used during the process of contact planarization (CP) using Computational Fluid Dynamics (CFD) software. This process, called CON-TACT[®] has been developed by Brewer Science, Inc. Rolla, MO. The variation of pressure on the optically flat plate with the solvent percentage in the polymer fluid is studied to find the optimum solvent percentage for the process. The fluid flow over the topography of the wafer is also studied.

This section gives an introduction to different wafer fabrication methods. Section 2 gives a brief introduction to CFD and the different techniques in solving an engineering problem in CFD and an overview of FLUENT[®] software. The CP process and the mathematical analysis of the model being used are explained in Section 3. The simulation procedure and the models being used in this project are outlined in Section 4.

1.2. INTRODUCTION

1.2.1. Wafer Preparation. Wafers play a very important role in the manufacture of semiconductor devices and integrated circuits and form the essential component of most electronic devices. Wafers, usually in micro-dimensions, are built on the surface of a substrate, on top of which the semiconductor devices are built. Silicon is the most commonly used substrate, and the wafers may contain multiple layers of different materials depending on their final usage. The thickness of each layer depends on the final application. Since the features of the wafer affect the performance of the electronic device, the wafer fabrication method is crucial.

The first step in wafer preparation is the growth of the semiconductor crystal, which is called the ingot. The first layer of the wafer is the substrate, which is obtained by slicing the crystal into the required thicknesses. The chip is then fabricated by layering, patterning, and doping the substrate. Patterning is the process of creating a pattern on the surface of wafer which involves both deposition and removal of materials in certain areas and is explained in Section 1.2.3. Doping involves the deposition of

materials to create the required patterning. For the formation of a semiconductor, materials like germanium and silicon are deposited. The substrate and layers may be single crystalline, poly-crystalline, or amorphous [1]. Surface properties such as roughness, uniformity, and chemical properties at the interface affect the fabrication process.

Figure 1.1 shows an example of a patterned wafer, which may be either circular or rectangular. Each square is called a die and contains different microchip patterns. The percentage in each of them indicates the density of features in that die. The thickness of a typical wafer varies from 10-12 μm in which each layer thickness can vary from 0.1-2 μm [1].

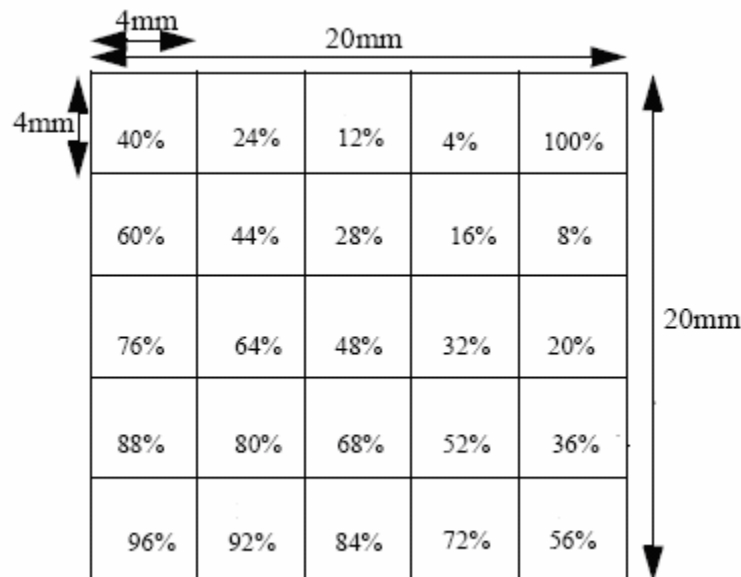


Figure 1.1 Density Variations in a Wafer [2]

Wafers are processed by a series of chemical and lithographic steps to produce integrated circuits (IC's) which are the main components of all electronic devices. They may be used as image sensors in automobiles and as memory chips in cell phones, computers, cameras, and digital audio players. In the medical field, they are used as both

image sensors and memory devices. They also have a wide range of applications in security systems as they can be used as image sensors in security cameras and surveillance units [3].

1.2.2. Fabrication Techniques for Patterning. Patterning involves modifying the shape of an existing layer. The existing layers must be patterned to tailor the wafer for the final usage. For example, the formation of a semiconductor on a surface requires the removal and deposition of different materials. P-type and N-type semiconductors are obtained by the addition of certain materials which increase the charge carriers. If the positive charge carriers are increased, it is called a P-type material and if the negative charge carriers are increased, it is called an N-type material. If the top layer is an N-type material, part of it must be removed and a P-type material must be deposited in that region in order to form a P-N junction. The process of marking and removing zones is called patterning, which includes methods like photolithography and etching.

1.2.2.1 Photolithography. The development of semiconductor technology requires the development of images in micro or nano-dimensions. This finds applications in semiconductor manufacturing and micro-electro-mechanical systems (MEMS), which involve the integration of mechanical and electrical elements onto the surface of a substrate. Photolithography is a technique used in micro-fabrication to remove selective parts of a given layer by using light. The first step of photolithography is coating the wafer with a photoresist. A photoresist is a substance which changes its structure and properties on exposure to light. Photoresists may be either negative or positive [5]. Negative photoresists change from a soluble (polymerized form) to insoluble state (unpolymerized form) and positive photoresists work in the opposite way. Photoresists usually have very high viscosity, so they are difficult to coat on the surface of the wafer. To overcome this difficulty a solvent is usually added to the photoresist before the coating step and evaporated later. The various deposition techniques are described in Section 1.2.4. After the coating is done the wafer is subjected to a soft-bake process where the solvent is partially evaporated.

The next steps for the photolithographic process are described in Figure 1.2. Figures b-d include those of a negative photoresist and Figures e-g are those of a positive photoresist. Once the photoresist is coated on the surface of the wafer, a mask is

prepared for patterning. The hard copy of the pattern is transferred on to the surface of a glass where the pattern is deposited by a layer of chrome (shown by the black block in Figure 1.2a). The glass with the pattern, called the mask, is placed on the wafer and then UV light is passed through it. The light reaches the surface of the wafer through the glass only at the regions which are not blocked (Figure 1.2a). The exposed parts of the photoresist will now have different properties than the unexposed parts. All the steps up to this point are the same for both negative and positive photoresists. For a negative photoresist, the unexposed parts, which are in the polymerized form, are removed by treating them with a chemical solution; the wafer is then subjected to a hard bake process where the remaining solvent is also evaporated. The wafer layer below the resist is removed through the opening in the resist layer (Figure 1.2c). Finally, the photoresist layer is removed. In the case of a positive photoresist, the unexposed regions are in an insoluble form and can be removed by treating them with a chemical solution. Then the top wafer layer is also removed in the regions where there is no photoresist and the photoresist layer is stripped off. The wafer obtained by either of these two processes may be doped with some other materials for the addition of an electric circuit [5].

1.2.2.2 Etching. Etching is the process of removing a portion of a layer on the surface of a wafer. Usually after the photolithography process, the resist layer is removed. The layer below, which is usually an oxide, must be removed only in the area where the resist is removed. Only the oxide in these regions must be removed, and if too little or too much is removed it is called over and under-etching, respectively (Figure 1.3). Under or over-etching changes the required dimensions of the wafer, which may result in the wafer not functioning properly.

There are two types of etching processes [1]: wet etching and plasma etching. Wet etching involves a chemical solution whereas plasma etching (also known as dry etching) makes use of a gas. Wet etching involves the immersion of the wafer in a chemical bath where the top layer of the wafer is removed by chemical reaction. The solution used for etching depends on the oxide layer being etched. If the top layer is silicon oxide, hydrofluoric acid is typically used. This process may be limited by the reaction or by the diffusion of the components.

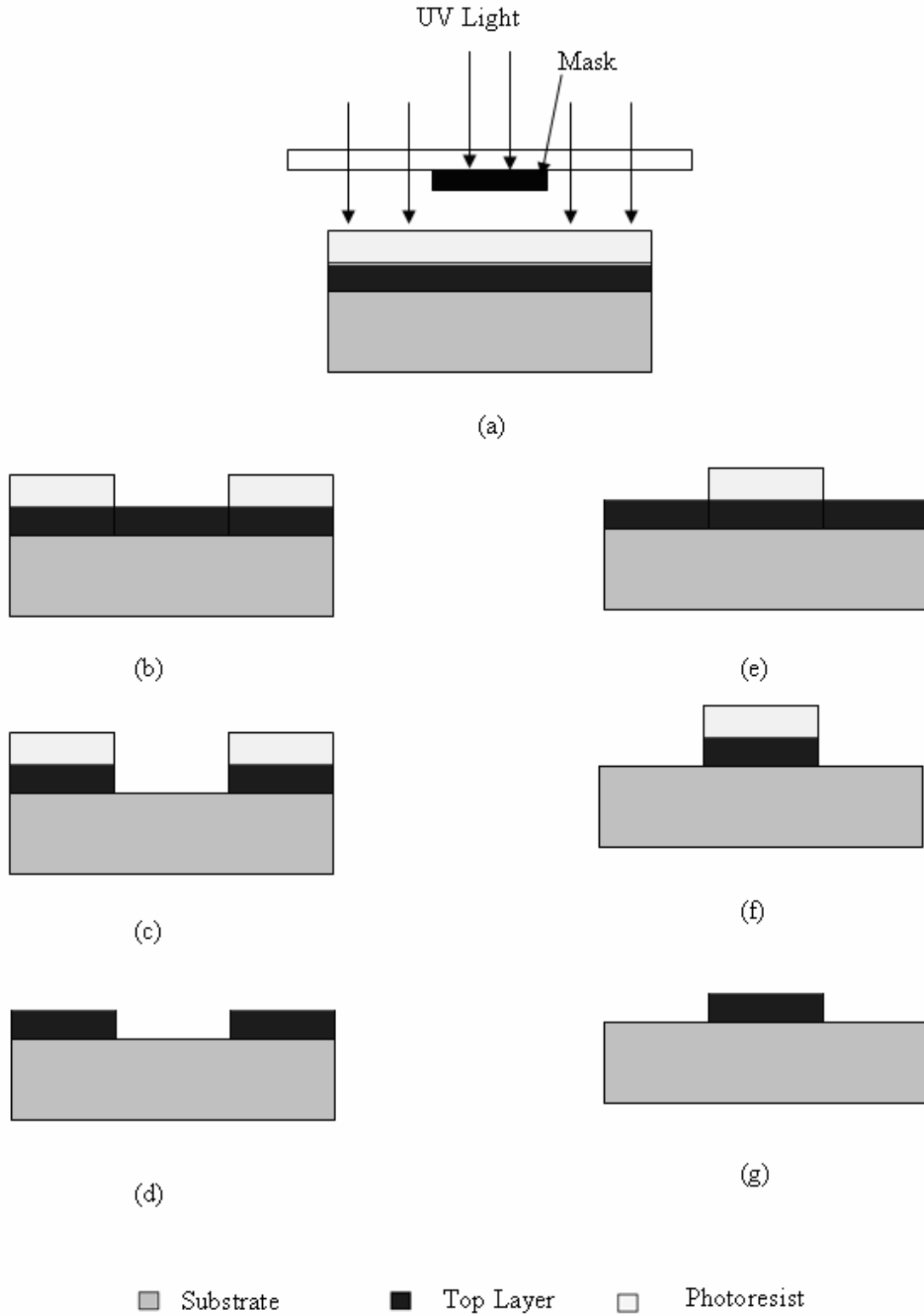


Figure 1.2 Photolithographic Process, (a) Mask Blocking UV Light, (b-d) Negative Photoresist Process, (e-g) Positive Photoresist Process

Plasma etching involves the passage of a gas through a vacuum chamber in which the wafers are placed. This gas is then energized by the application of electrical energy. The gas reacts with the wafer layer to produce volatile compounds which are removed by vacuum. For the removal of silicon dioxide on the wafer, a mixture of CF_4 with oxygen is used [5].

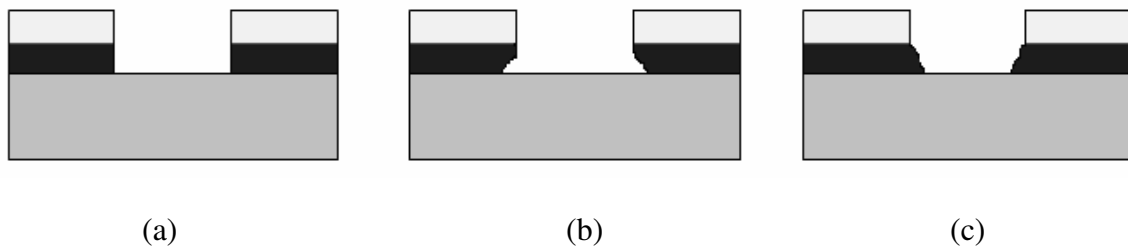


Figure 1.3 Degree of Etching, (a) Proper Etching, (b) Over-Etching, (c) Under-Etching

1.2.3. Fabrication Techniques for Layering. To develop electric circuits on the surface of a wafer, different materials have to be deposited on its surface. An electric circuit consists of different units such as N-P junctions, transistors, and capacitors. If a semiconductor is to be formed, a P-type or N-type has to be deposited on its surface. Some regions of the already existing layer have to be etched and the corresponding material has to be deposited on the surface of the wafer. For an N-P junction to be formed, another oxide layer must be deposited in this region. An N-P junction is the junction between two types of semiconductor materials (P-type and N-type). Similarly, several other electrical units such as insulators and conductors are built on the wafer.

The construction of all these devices on the wafer surface needs the deposition and etching of several kinds of materials. There are different deposition techniques, including physical vapor deposition (PVD), chemical vapor deposition (CVD), sputtering, evaporation, epitaxy, electrochemical deposition, and spin-coating. The properties of a given layer will be different if deposited by two different methods. In addition, the process conditions of the deposition technique change the properties of the

deposited layer. For example, it has been found that the properties of a molybdenum layer, such as resistivity, change for different sputtering process conditions [1]. Process conditions like temperature also affect the properties of the layer. For example, temperature affects the crystalline nature of the layer [1]. The process conditions and the deposition technique are chosen based on the properties required for the electrical circuit.

In physical vapor deposition, the target metal is excited and the vapor atoms are transported to the surface of the substrate in vacuum. The excitation can be achieved by different techniques, including arc vaporization and ion bombardment. This method is mostly used for thin-film deposition. Since the vapors are produced by a physical source it is called PVD. Sputtering is a type of PVD in which the target is bombarded with argon plasma which results in the ejection of target atoms, which are then deposited onto the surface of the substrate. The advantage of this method over the other methods is the production of a layer of the same composition as the target material [1]. Evaporation is another process used for thin film deposition where the source material is evaporated in vacuum, and the vapors are deposited on the surface of the substrate. The quality of the layer depends on the purity of the sample and quality of the vacuum. Some foreign particles may be left behind if vacuum is not applied properly. These may react with the gaseous source reducing the number of gaseous atoms reaching the substrate surface. On the other hand, if two or more gases are passed over the substrate to form a layer on it, it is called CVD [6]. The reactant gases may decompose or react and the product is deposited on the surface of the wafer. The CVD process may take place at atmospheric and low pressures or even at vacuum.

Epitaxy is the process of growing a crystalline structure on the surface of the substrate. In this process the crystalline structure is taken from the layer below. Molecular beam epitaxy (MBE) is a type of epitaxy where evaporation of the source takes place in vacuum. The difference between MBE and evaporation is that the source is evaporated in a crucible with a small opening. In electrochemical deposition, the wafer to be coated is used as a cathode and the source metal is an anode [7]. When these electrodes are connected in a circuit, the metal is deposited on the surface of the wafer.

Spin coating is mostly commonly used for coating of photoresists [1]. In this method, the wafer is first mounted onto the surface of a spinning table and a few

milliliters of resist are placed at the center of the wafer. The slow rotation of the table allows for spreading of the resist. After the resist reaches a specified diameter, the acceleration of the spinning table is increased. Centrifugal force throws excess material off the wafer thus eliminating accumulation along the edges of the wafer. Higher acceleration also helps to evaporate the solvent and thus provides good binding with the wafer. The spin processes may be either manual or automatic. The advantages of this process are that it covers any pin holes in the lower layer, and a small of quantity of coating fluid is needed. This method is very useful for multi-layer applications [8].

1.2.4. Need for Planarization. Microstructure manufacture is a crucial step for semiconductor devices. In wafer manufacturing, some layers do not extend over the whole surface but are confined to a few regions, such as in the construction of semiconductor devices on a circuit. When a layer is fabricated, the topography of the layer below it is carried upward, as can be seen in Figure 1.4. The conformation to topography increases with the number of layers being applied on the microstructure. The photoresists used in photolithographic processes change their shape when the solvent is evaporated. At higher temperatures, the solvent has the ability to flow, changing the shape and dimensions of the structures on the layer as shown in Figure 1.5. A significant change in the topography also limits the number of layers that can be fabricated successfully [9].

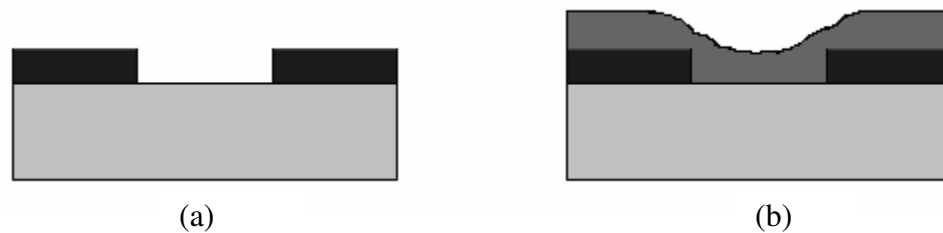


Figure 1.4 Topography Conformation, (a) Top Layer of the Wafer Showing the Topography, (b) New Layer Showing the Conformation to Topography

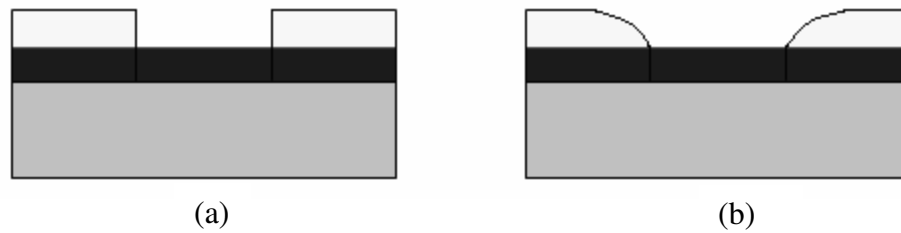


Figure 1.5 Change in Shape of the Photoresist, (a) Room Temperature, (b) After Solvent Evaporation

There are different definitions used to qualify planarization, including local and global planarity, aspect ratio and degree of planarization. Surface planarization may be either local or global. Local planarity is also known as short range planarity. If a wafer is said to be locally plane, it might be perfectly flat within a particular zone but may not be flat when compared with the whole surface. On the other hand, global planarity indicates uniform thickness across a particular die. Aspect ratio is the ratio of the height of the layer over the topography after planarization (T_p) to the normal height of the topography before planarization (T_h) (Figure 1.6). Degree of planarization (DOP) is defined by the following formula [10]:

$$\text{DOP} = 1 - T_p / T_h \quad 1.1$$

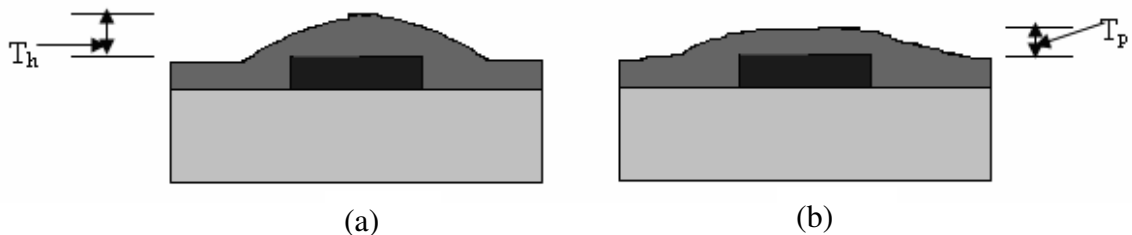


Figure 1.6 Height over Topography, (a) Before Planarization, (b) After Planarization

The photolithographic steps described in Section 1.2.2.1 require planarity of the wafer as they can be used to transfer an image only to a perfectly plane surface. If the surface is not flat, the image will be blurred. The resolution, W , of an image produced by lithography is defined by the following equation [11]:

$$W = \frac{k_1 \lambda}{NA} \quad 1.2$$

where k_1 is a constant for a specific lithographic process, λ is the wavelength of the optical tool, and NA is the numerical aperture of the optical tool.

The resolution can also be defined as the minimum feature size that can be produced by a particular process. According to Equation 1.2, the minimum feature size can be increased either by decreasing the wavelength or increasing the NA of the tool, but these factors affect the depth of focus (D) of the device, which is defined as the distance from the lens in which the image will be in focus, and is given by the following equation [11]:

$$D = \frac{k_1 \lambda}{NA^2} \quad 1.3$$

Equation 1.3 shows that decreasing the wavelength or increasing the NA of the optical tool decreases the depth of focus of the image. This demands the application of a thin, planar layer of photoresist in photolithographic processes.

1.2.5. Planarization Techniques. Planarization processes are required to produce smooth and flat surfaces by eliminating rough topographies and thus helping in proper image transfer. There are many planarization techniques [12], including chemical-mechanical, etch-back, chemical, and spin etch planarization, of which the most commonly used technique, chemical-mechanical planarization, is explained in this section.

1.2.5.1 Chemical-mechanical planarization. Chemical-mechanical planarization (CMP) is a process used to planarize metal and dielectric surfaces. This process makes use of both chemical and mechanical forces to planarize the surface. The main components of this process are chemical slurry, polishing pad, and the wafer surface to be planarized [13]. Figure 1.7 shows the setup of a typical CMP process.

The wafer and the polishing pad are rotated in opposite directions. The chemical slurry contains abrasive particles which react with the wafer material. Since mechanical forces are applied to the wafer, the material in higher regions is subjected to greater mechanical forces and is removed much faster than those in the lower regions, thus creating a planarized surface. The speed of the pad can be optimized to obtain maximum planarization and to minimize the pressure on the surface. Advantages of this method are that it provides global planarity and can be used with many materials [14]. Apart from these advantages, there are many disadvantages to this method, including potential contamination of the clean-room environment by the chemical slurry. As this method is used for dielectrics, dishing or erosion may occur (Figure 1.8). Dishing occurs when the dielectric is removed at a faster rate than the underlying structure. Erosion occurs when the material (both the dielectric and the underlying structure) in one area is removed faster than that in other areas. Another disadvantage is that the density of the underlying structure also affects the performance of CMP, called the feature density effect [12].

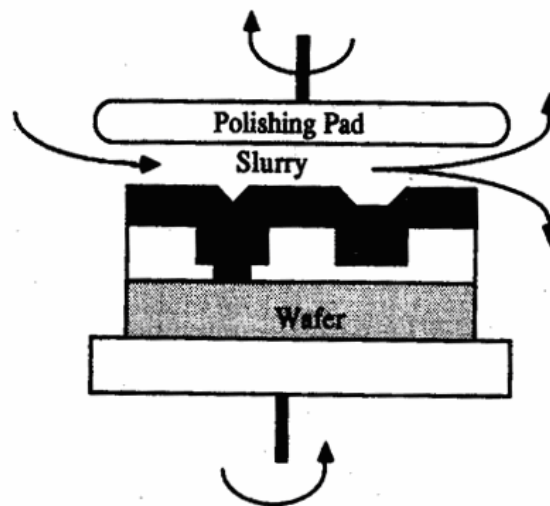


Figure 1.7 Setup for CMP [5]

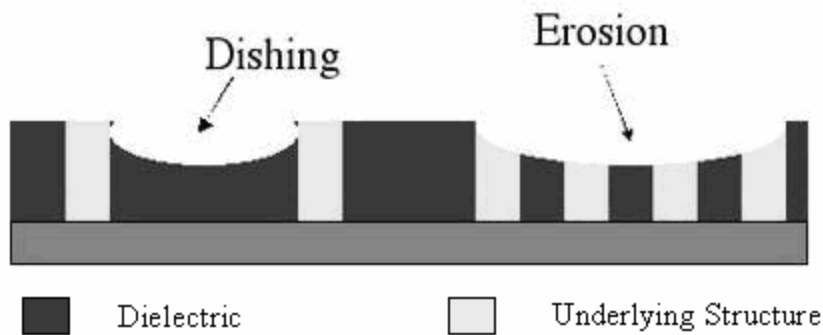


Figure 1.8 Dishing and Erosion [12]

1.2.5.2 Etch-back planarization. In the process of etch-back planarization, a more planar layer is applied onto the surface having topography. This is done by spin coating a planarizing material which has a low viscosity. If the etch rate of both the wafer and the overlying material are similar, then etching can be used to remove the planarizing material and to transfer its surface planarity to the wafer's surface. Studies have indicated that this method has provided only an average of 55% degree of planarization [15]. This is due to the lack of planarizing materials which can provide a perfectly flat surface.

1.2.5.3 Contact planarization. Contact planarization (Figure 1.9) is an alternative method to CMP developed by Brewer Science, Inc. In this method, a dielectric is deposited onto the wafer surface containing the topography. When this dielectric is in a flowable state, the wafer is pressed against an optically flat surface whose flatness is transferred to the wafer's surface. This is left in contact with the surface for a sufficient time and then removed. This method provides both global and local planarity and eliminates the use of chemical slurries which can contaminate the clean room environment.

To avoid the feature density effect, a sacrificial material is first spun onto the surface of the wafer. If the viscosity of this material is very high, a solvent is added to make it easier to spin. After it is spun, a residual amount of solvent is evaporated such that the material is in a flowable state. Then the wafer is brought into contact with an

optically flat surface in vacuum and the material is cured with UV light to evaporate the remaining solvent and to harden the material. After some time, the wafer is separated from the flat surface and the sacrificial material whose surface is flattened is etched. The wafer surface is then etched to the desired thickness. In this way the planarity is transferred from the optically flat surface to the wafer.

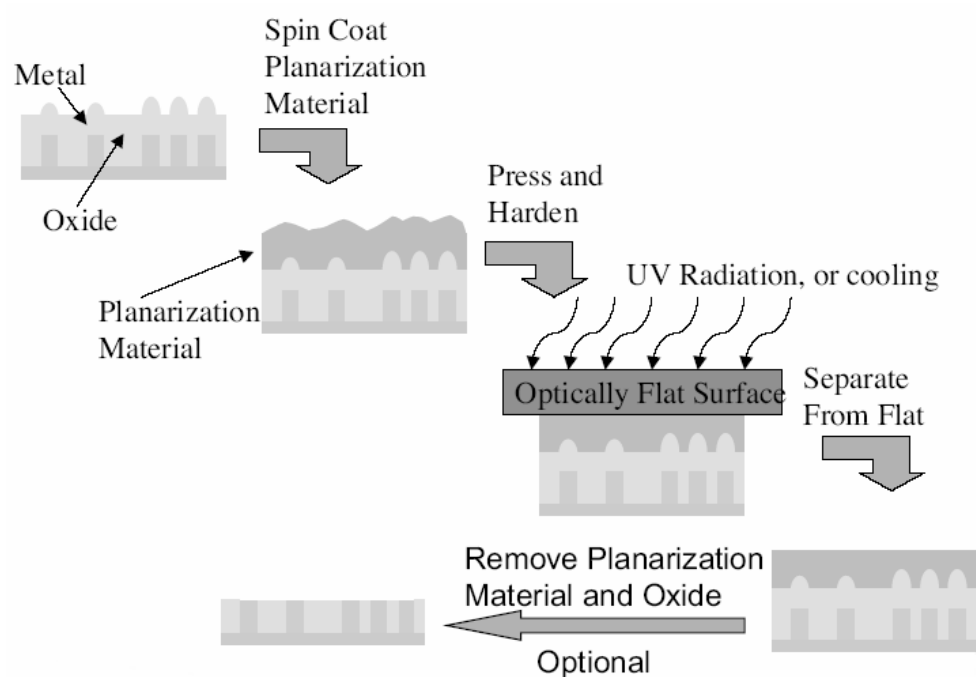


Figure 1.9 Contact Planarization Process [16]

Contact planarization process takes place in a chamber called a CON-TACT planarization tool. This contains an optically flat surface below which is a provision for placing the wafer. The wafer can be raised to touch the flat surface. The optical surface is transparent to allow UV radiation to pass through. A specified pressure can be applied onto the surface of the wafer by the flat surface. The wafer is left in the chamber for a specified period of time to make the wafer as flat as possible.

2. INTRODUCTION

2.1. INTRODUCTION TO CFD

Computational Fluid Dynamics (CFD) is a technology to study the dynamics of flow mathematically. CFD bridges the gap between pure theory and pure experiment and provides a third approach to solve fluid dynamics problems, but cannot replace either of them as pure theory and experiment are required in the analysis of results. CFD utilizes computational power to perform numerical calculations, so the results can be interpreted without actually conducting experiments, reducing cost and time. It aids in the virtual reconstruction of a system and applies real-world physical and chemical principles to study the system behavior, as well as quantitatively predicting profiles of velocity, pressure, temperature, and other process variables. CFD has applications in many fields including fluid mechanics and aeronautical, mechanical, chemical, and metallurgical engineering.

2.2. NEED AND HISTORY OF CFD

The major storm and fire disaster which occurred in Britain in 1987 [17] caused much damage to life and property. The storm was predicted by many other countries that made use of computers to forecast wind speed and direction. By predicting the storm, Britain could have reduced the damage. No evidence exists as to why Britain did not predict it, or why other countries did not provide Britain with a warning. In cases like this, there is a need to predict the flow of fluids by solving the physical governing equations. These equations are coupled and are relatively difficult to solve, so the use of computers to solve them was the basis for the development of CFD. The contributions to theoretical fluid dynamics started in the late 17th century by the introduction of Newton's Laws of Motion. Further significant work was done in the 18th and 19th centuries when the Navier-Stokes and Euler equations were derived. The first complex fluid dynamics calculations were solved by hand by Richardson in 1910 and included about 2000 operations every week [18]. Though the time at which CFD started is debatable, the use of commercial code started around the 1980's [17].

CFD provides an alternative method for studying actual processes without actually performing them or doing pilot plant experiments. For example, it is very difficult to create environments at extremely high Mach numbers or temperatures, so experiments on aeronautical vehicles benefit from simulated flow profiles in CFD. CFD also helps to study flow properties non-invasively, and allows researchers to study process variables at inaccessible locations, such as inside a hot furnace. Carrying out test simulations can also reduce the number of designs to be tested experimentally for final inspection.

2.3. GOVERNING EQUATIONS OF CFD

The basic governing equations for any single phase, non-reacting fluid flow process are the Navier-Stokes equations, i.e., conservation of mass and momentum. The conservation of energy is solved only for temperature dependent processes. Based on the different models chosen for solving the problem, the corresponding equations are solved. For example, k- ϵ or one-model equations are solved for turbulent systems and the multiphase equations, such as volume of fluid equations, are solved for multiphase models. If the flow involves complexities such as non-Newtonian fluids or flow with chemical reactions, the corresponding equations are added and solved to give the process values. These equations may be either in the conservative (containing partial derivatives) or non-conservative form (containing integrals).

The complete Navier-Stokes equations are listed as Equations A.1-A.10 in Appendix A. These equations include all the terms due to viscous, inertial, and body forces. If the viscous forces are small compared to the inertial forces, the flow is inviscid, and the Navier-Stokes equations are modified to obtain the Euler equations for inviscid flow, where the viscous terms are neglected. The Euler equations are listed as Equations A.11-A.20 and include the continuity, momentum, and energy equations, both in the conservative and non-conservative forms [19].

For a given system, the corresponding set of equations is solved to give the solution profile. Before solving, they are modified by a process called discretization. The discretization procedure and the various techniques are discussed in the following sections.

2.4. PROBLEM SOLVING TECHNIQUES

2.4.1. Problem Setup. The first step in solving any mathematical problem is to set up the problem statement. This can be illustrated by considering examples of water flowing through a pipe and over a flat plate. The Navier-Stokes equations are solved to obtain the flow profiles for both cases, but the differences are introduced through the boundary conditions. Flow through a pipe involves a system confined by walls on all sides. Flow over a flat plate is only confined by one wall, and the top boundary is open to the atmosphere. Before solving a problem, the problem statement and operating conditions should be very clear for choosing the discretization schemes and convergence criteria. After the problem statement has been defined, the geometry of the computational domain is created and the boundary conditions are specified.

2.4.2. Discretization. The computational domain obtained in the previous step is a continuous one, and the process values and flow variables are defined at each point in the domain. This continuous domain must first be converted to a finite one, where the properties are defined at discrete points (nodes) rather than throughout the whole domain. This process is called discretization, mostly commonly referred to as meshing. The governing equations either in conservative or non-conservative forms are converted to a set of algebraic equations. The original equations defined over the whole domain are converted to another form which can take values from the discrete points. These equations obtained after discretization are called discrete equations and are solved to give the flow profile. There are several discretization techniques, of which the most commonly used are finite difference (FD), finite volume (FV), and finite element methods (FE). Different software packages use different discretization techniques.

2.4.2.1 Finite difference method. The finite difference method is used to determine process variables by calculating a finite difference quotient calculated using Taylor series. This method is based on the process values at discrete points called nodes. A schematic representation of the nodes is shown in Figure 2.1. The value of the derivatives in the governing equations are calculated individually and then substituted to solve the governing equations to solve for the process values. The Taylor series expansion for velocity is given below:

$$u_{i+1,j} = u_{i,j} + \left(\frac{\partial u}{\partial x}\right)_{i,j} \Delta x + \left(\frac{\partial^2 u}{\partial x^2}\right)_{i,j} \frac{(\Delta x)^2}{2} + \left(\frac{\partial^3 u}{\partial x^3}\right)_{i,j} \frac{(\Delta x)^3}{6} + \dots \quad 2.1$$

where 'u' represents the velocity at a point and i and j indicate the x and y directions, respectively. The distance between two consecutive nodes in the x-direction is Δx and in the y-direction is Δy , which may be equal depending upon the domain.

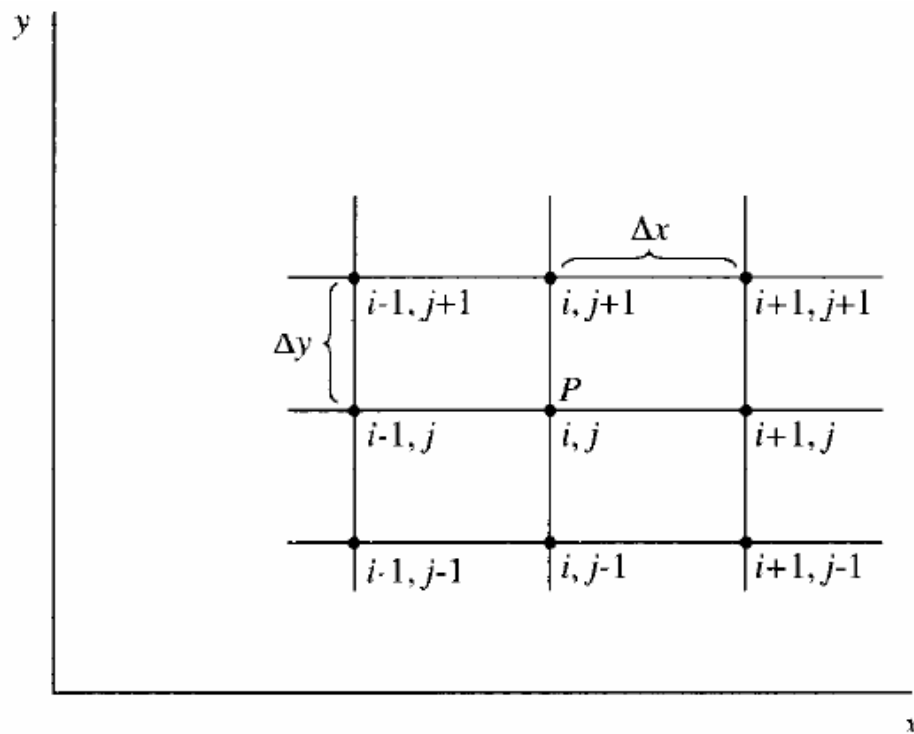


Figure 2.1 A Grid Showing the Discretization Procedure [19]

There are eight neighboring nodes at discrete distances to the node P. The governing equations contain derivatives of the flow variables. The numerical values of the derivatives are needed to solve the governing equations. If the velocity at node P is known from the initial or boundary conditions the values at the neighboring nodes can be calculated by the forward, backward, or central difference formulas [19]. These formulas are based on flow from left to right.

Forward difference:

$$\left(\frac{\partial u}{\partial x}\right)_{i,j} = \frac{u_{i+1,j} - u_{i,j}}{\Delta x} + O(\Delta x) \quad 2.2$$

$$\left(\frac{\partial u}{\partial y}\right)_{i,j} = \frac{u_{i,j+1} - u_{i,j}}{\Delta y} + O(\Delta y) \quad 2.3$$

In the above formulas, the value of the derivative $\left(\frac{\partial u}{\partial x}\right)$ is calculated based on the velocity at P $(u_{i,j})$ and the node next to it $(u_{i+1,j}, u_{i,j+1})$, so it is called the forward difference method. The terms $O(\Delta x)$ and $O(\Delta y)$ indicate all the other terms in the Taylor series expansion. This term is called the truncation error and is usually neglected in the actual calculations. The lowest order term in $O(\Delta x)$ gives the order of the formula; for example, since the above formula includes Δx , it is called first order forward difference.

Backward difference:

$$\left(\frac{\partial u}{\partial x}\right)_{i,j} = \frac{u_{i,j} - u_{i-1,j}}{\Delta x} + O(\Delta x) \quad 2.4$$

$$\left(\frac{\partial u}{\partial y}\right)_{i,j} = \frac{u_{i,j} - u_{i,j-1}}{\Delta y} + O(\Delta y) \quad 2.5$$

Since the derivative in the above formulas is calculated based on the velocity at P and the velocity at the node before it $(u_{i-1,j}, u_{i,j-1})$, it is called backward difference. This is also of first order as the formula contains $O(\Delta x)$ and $O(\Delta y)$.

Central Difference:

$$\left(\frac{\partial u}{\partial x}\right)_{i,j} = \frac{u_{i+1,j} - u_{i-1,j}}{2\Delta x} + O(\Delta x)^2 \quad 2.6$$

$$\left(\frac{\partial u}{\partial y}\right)_{i,j} = \frac{u_{i,j+1} - u_{i,j-1}}{2\Delta y} + O(\Delta y)^2 \quad 2.7$$

The central difference formula calculates the derivative based on the velocities at nodes before $(u_{i-1,j})$ and after P $(u_{i+1,j})$. The value at point P can be calculated using any

of the above formulas depending on the available boundary conditions. If the above formulas are used for unstructured meshes then relevant transformations must be included.

2.4.2.2 Finite volume method. The finite volume method is used to evaluate the values of partial derivatives. The basic element used for calculation is the small volume around the node in the mesh. The terms in the governing equation are first integrated over the whole volume and the volume integrals are replaced by surface integrals using the divergence theorem. The terms in the equation are then calculated by evaluating the surface fluxes on the faces of the volume which are based on the FD formulas. This method is an advanced method to FD method. The discretization formulas used in this method can be derived via the formulas in the FD method [20]. This method can also be used for situations where discontinuities arise, which causes the FD method to fail [21]. The advantage of the FV method over the other methods is that it can be used for unstructured grids as well.

2.4.2.3 Finite element method. The finite element method is used to solve partial differential and integral equations and is based on the properties of discrete elements which constitute the domain. The solution procedure involves the following steps [21]:

- The domain is first divided into a finite number of sub-domains, where each sub-domain is called an element, and the overall domain is called a finite element mesh. The mesh may be either uniform or non-uniform depending on the geometry. For example, to calculate the circumference of a circle, the figure is divided into a number of finite elements denoted by the straight lines in Figure 2.2. The elements may or may not be uniform.
- The governing equations are then converted in terms of the element properties. In this case, the governing equation is the equation for the circumference of a circle. In the approximation using a finite element method, the length of each element is calculated by the following equation.

$$l_i = 2R \sin\left(\frac{\theta}{2}\right) \quad 2.8$$

Similar equations are written for all the elements in the domain and are called element equations [21]. After solving the element equations, the process variables for the corresponding elements are obtained.

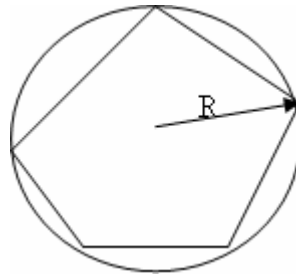


Figure 2.2 Elements on the Circumference of a Circle

In Figure 2.3, the length of the arc subtended by the sector OAB can be calculated, because the radius and the angle ' θ ' are known.

- The approximate value of the process variable over the whole domain is obtained by combining the elemental values in a relation which is given by the geometry. The circumference of the circle is obtained by adding up the length of all the elements. It can be seen that if finer elements are used, the approximated value will approach the actual value of the circumference.

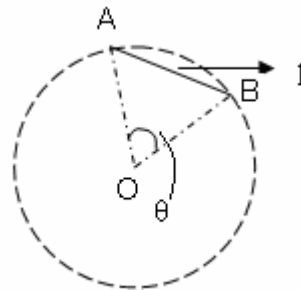


Figure 2.3 Circle Indicating the Elemental Properties

All these techniques provide an approximate solution because in the calculation of the variables, the higher order terms are neglected. This gives a deviation from the actual value. The solution accuracy is independent of the method but dependent on the grid formulation.

2.4.3. Solver Formulation. The solver is chosen based on the problem being solved which may be at either steady or unsteady state. Models specifying conditions applicable to the given problem, such as laminar or turbulent flow, multiphase systems, heat transfer, and mass transfer are selected in this step. For each of the models chosen, the corresponding equations are discretized by any of the above methods and solved. The model applicability depends on the software being used, and some have broader ranges than others.

2.5. SOLUTION CONVERGENCE AND ITERATIONS

Discretization produces a set of equations which must be solved for the process values across the whole domain. These equations can be solved directly or by using iterative methods. Direct methods require more computation [23] because additional grid points must be used for better accuracy, which further increases the level of computation. This effort is much less for iterative processes, especially for 3-dimensional problems. A general method for solving equations using iteration is described by Kreyszig [23]. Gauss-Siedel and Jacobi methods are some of the commonly used iterative methods. The solution is said to be converged when the difference between the process values obtained at two consecutive iterations is less than a residual amount which can be set by the user.

For steady state problems, the equations are solved and the values are updated during each iteration. For transient problems, the process values at a particular time-step are calculated from previous ones. The discretized equations for the time-dependent process may be solved either explicitly or implicitly. An explicit process involves the calculation of process values using the values only from the previous time-step. An implicit method produces a set of equations which contain variables from the current time-step and process values from the previous time-step. The implicit method requires more computation.

2.6. CFD TECHNIQUES

Some problem-solving techniques are applicable only to a particular genre of problems. One such technique is the relaxation technique which can be used only for solving elliptic partial differential equations, such as low speed subsonic flow equations [19]. The classification of partial differential equations is described by Kreyszig [23]. The relaxation technique uses the finite difference method and may be either explicit or implicit.

Another technique which can be used to solve the Navier-Stokes equations is the pressure correction technique, which involves the calculation of a guess velocity field based on the guess pressure. The corrected pressure is then obtained from the continuity equation and the velocity field values are updated based on the new pressure. The pressure correction algorithm for engineering problems, called SIMPLE, is explained by Patnakar and Spalding [25]. Some other pressure correction techniques include SIMPLER, SIMPLEC, AND PISO [26]. For inviscid and incompressible flows where the governing equation is elliptic, both relaxation and pressure-correction techniques must be used.

The adaptive grids technique has increased the problem solving capability of CFD. This technique can be used to provide more refined mesh or closely located nodes in the region where there are large gradients. This method provides better accuracy in calculating the high gradients. The method to find the flow profile in a boundary layer is given in Figure 2.4.

In Figure 2.4a, it can be seen that the nodes are far from the boundary layer. In order to obtain better accuracy, the grid near the boundary layer is adapted. This produces a new grid in which the nodes are closer to each other near the area of interest and move farther apart away from the boundary layer. In cases where cylindrical or spherical coordinates are used, the governing equations may be transformed into the corresponding variables. There are cases where it might be required to use a special kind of transformation to make the computation easier. In these cases, specific transformation formulas are used to transform the equations as well as the grid in terms of the transformed variables. An example of such a transformation is required in the flow in a

duct, which is shown in Figure 2.5. The curvilinear coordinates are converted to rectangular coordinates using the following transformation [19]:

$$\xi = x \quad 2.9$$

$$\eta = y/y_s \quad 2.10$$

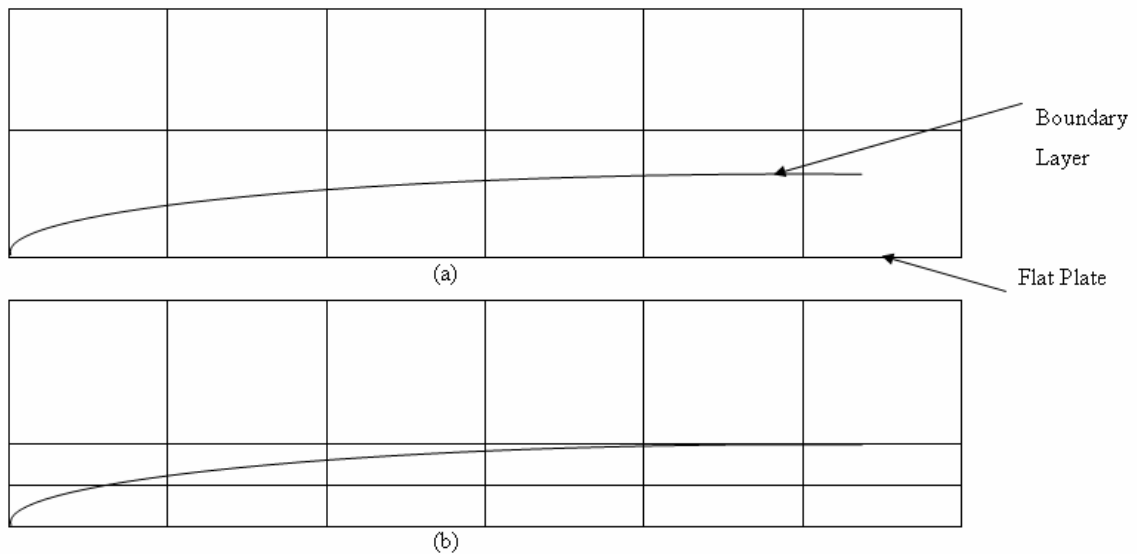


Figure 2.4 Grid for Flow Past a Flat Plate, (a) Uniform Boundary Layer Grid With Equal Spacing, (b) Adapted Grid of the Boundary Layer [19]

2.7. POST-PROCESSING

Once the equations are solved to obtain the flow variables, they need to be analyzed to see if they meet the requirements of the process such as uniform temperature or velocity profiles. There are several kinds of plots in CFD analysis, some of which are listed below.

XY Plot: An XY plot can be used to see the variability of one parameter with respect to another. These plots are easier to read as they are very simple and the relation between any two variables can be understood; for example, the x-velocity over the length of a pipe can be studied. Figure 2.6 is an example of an XY plot which shows the

relation between gas velocity and the axial coordinate, and it can be clearly seen that the gas velocity decreases with the axial coordinate.

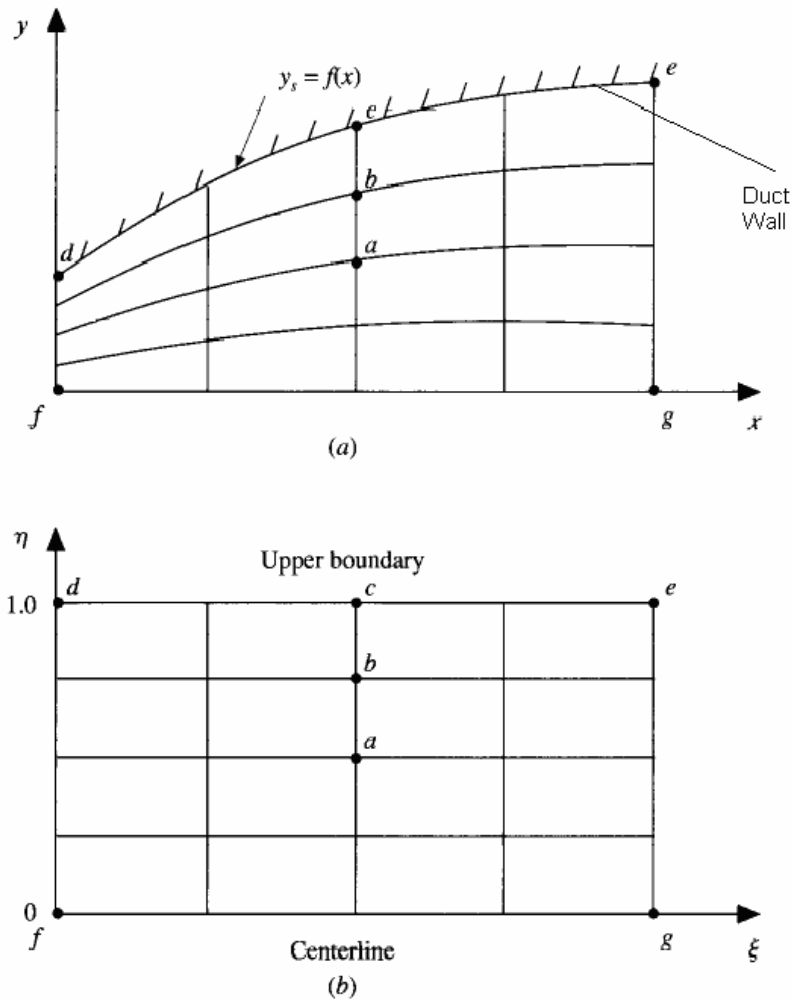


Figure 2.5 Grid of a Duct [19],
 (a) Physical Plane, (b) Computational Plane

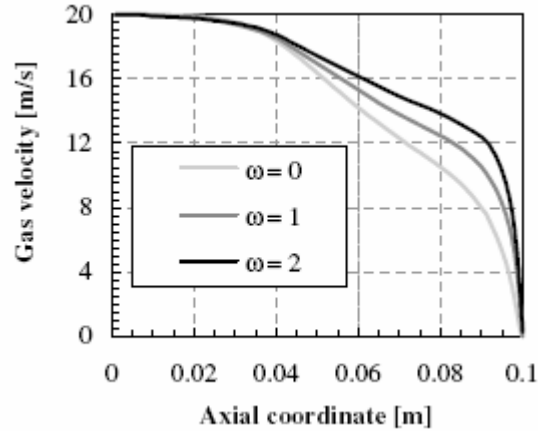


Figure 2.6 Example of an XY Plot [27]

Contour Plot: Contour plots represent the global nature of the variables and can be used for both vector and scalar quantities. A contour line represents a constant value of a particular variable. These figures are presented in such a way that the difference between adjacent contour lines is always constant. Figure 2.7 shows a contour plot of temperature in a mixing elbow. The temperature at any point in the flow domain can be determined from the scale on the left side of the plot.

Vector Plot: A vector plot gives both the direction and magnitude of the variables. The direction is notated by an arrow and the magnitude by color. As the name suggests, these types of plots can be used to represent only vector quantities. The flow profile of the solution in a fountain-plating system, which is used to coat wafers, is shown in Figure 2.8. The direction of flow is shown by arrows.

Streamline Plot: A streamline is a plot of the stream functions, which are mathematical substitutes for the velocity components given by Equations 2.11 and 2.12 [29]. Streamlines are tangential to the velocity vectors at each point. Figure 2.8 also shows the streamlines for the flow.

$$v_x = \frac{\partial \psi}{\partial y} \quad 2.11$$

$$v_y = -\frac{\partial \psi}{\partial x} \quad 2.12$$

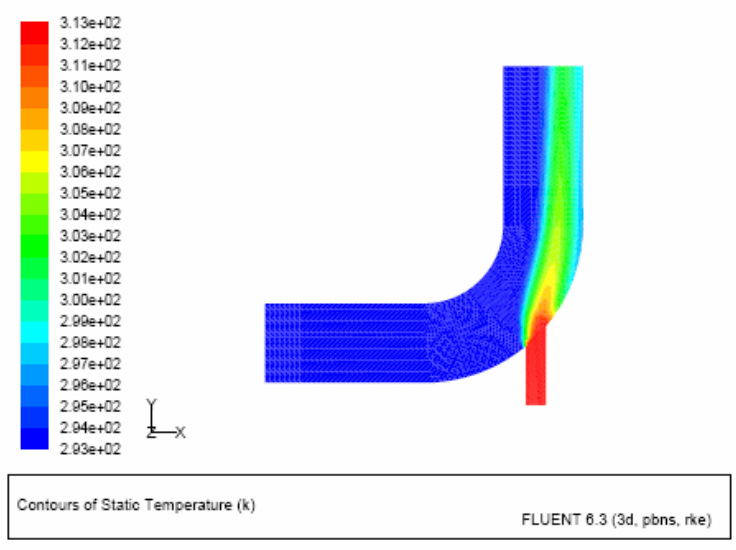


Figure 2.7 Example of a Contour Plot [18]

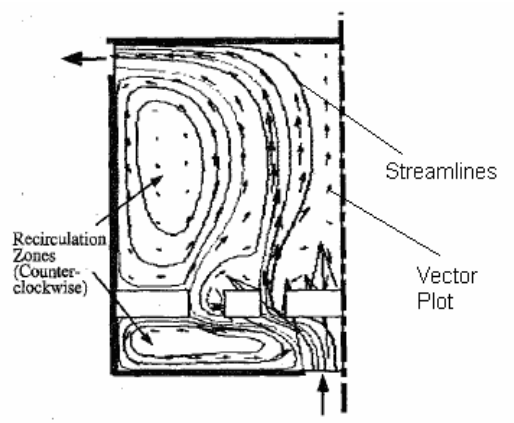


Figure 2.8 Example of a Vector Plot [28]

Scatter Plot: In a scatter plot, the magnitudes of the variables are denoted by symbols which are drawn at discrete points along the grid. These plots can be used for scalars whose magnitudes are indicated by size, shape, or color, but only the magnitude and not direction of vectors can be indicated. Figure 2.9 shows a scatter plot of y-velocity and density along a tube. The diameter of the circle indicates the velocity and

the shade of the circle indicates the density, which is usually indicated by a scale. Larger circles indicate higher velocities and darker circles indicate higher densities.

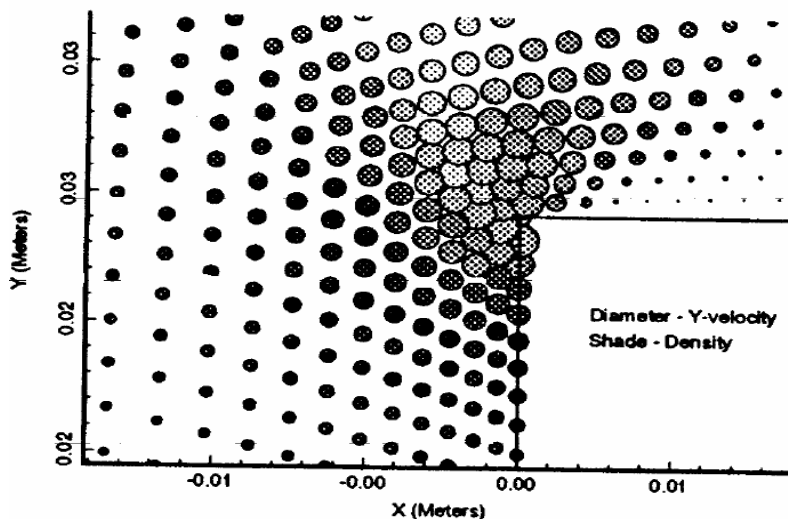


Figure 2.9 Scatter Plot of y-Velocity and Density Along a Tube [19]

2.8. OVERVIEW OF FLUENT SOFTWARE

2.8.1. Introduction. FLUENT was developed by Fluent Inc. (Lebanon, NH) and is a state-of-the-art computational tool that uses the finite volume method to solve fluid flow problems. It is a robust, reliable comprehensive CFD package. The FLUENT user interface consists of a Graphical User Interface (GUI) with pull-down menus and a Text User Interface (TUI) where commands can be specified to perform certain operations, such as saving a file, reading it back, and modifying the memory properties defined in the FLUENT manual [18].

2.8.2. FLUENT Modeling Examples. CFD is a developing field, but there have been satisfactory results for several engineering problems. There are a number of modeling examples using FLUENT, including the design of a mixing manifold of a Boeing aircraft, which saved approximately 75% of the total project cost by avoiding field work [30]. Another example is tank sloshing where Hadzic et al. [31] used the

volume of fluid (VOF) method to track the interface between two immiscible phases (air and water). They found that the amplitude and pressure results obtained from the simulations were in good agreement with experimental data.

Pantula performed a FLUENT simulation of water splashed by car tires and found results in good agreement with experimental data [19]. The experimental and simulation results of flow profiles of water and air in plate type heat exchangers done by Andersson [20] were in good agreement where the VOF method was used for the multi-phase model. Andersson also observed that the VOF method is unsuitable for multiphase flows when one of the phases has a very small volume fraction [20]. In the analysis of the performance of a reversible axial fan, Kokturk found that simulation results were in good agreement with experimental data for turbulent modeling [21].

2.8.3. Program Structure. The FLUENT [18] package includes a solver (FLUENT), preprocessors (GAMBIT, T-Grid, G/TURBO), and filters/translators (for importing meshes from other packages such as NASTRAN and AutoCAD). The organization of the above components and the interactions among them are shown in Figure 2.10.

The computational domain must be created before solving a problem. GAMBIT supports both 2D and 3D geometries and is used to create the geometry and define boundary types. The supported mesh types are triangular, quadrilateral, tetrahedral, hexahedral, pyramid, wedge, and hybrid, which are shown schematically in Figure 2.11. The mesh can also be refined or adapted depending on the problem requirement in FLUENT. The geometry is created and meshed, dividing the domain into discrete units.

The discretized computational domain is then exported to FLUENT where the models and process parameters are chosen. The standard interface may not meet the needs of all the problems, so user defined functions (UDF's), which are programs written by the user, can be hooked to FLUENT. In the example of a flow through a pipe, FLUENT allows the user to specify the inlet velocity. UDF's are used in this example if the flow is to be started after a certain amount of time or if the flow follows a specific profile. These are explained in detail in Section 2.9.8. Some of the modeling capabilities in FLUENT 6.2 are listed in the next section.

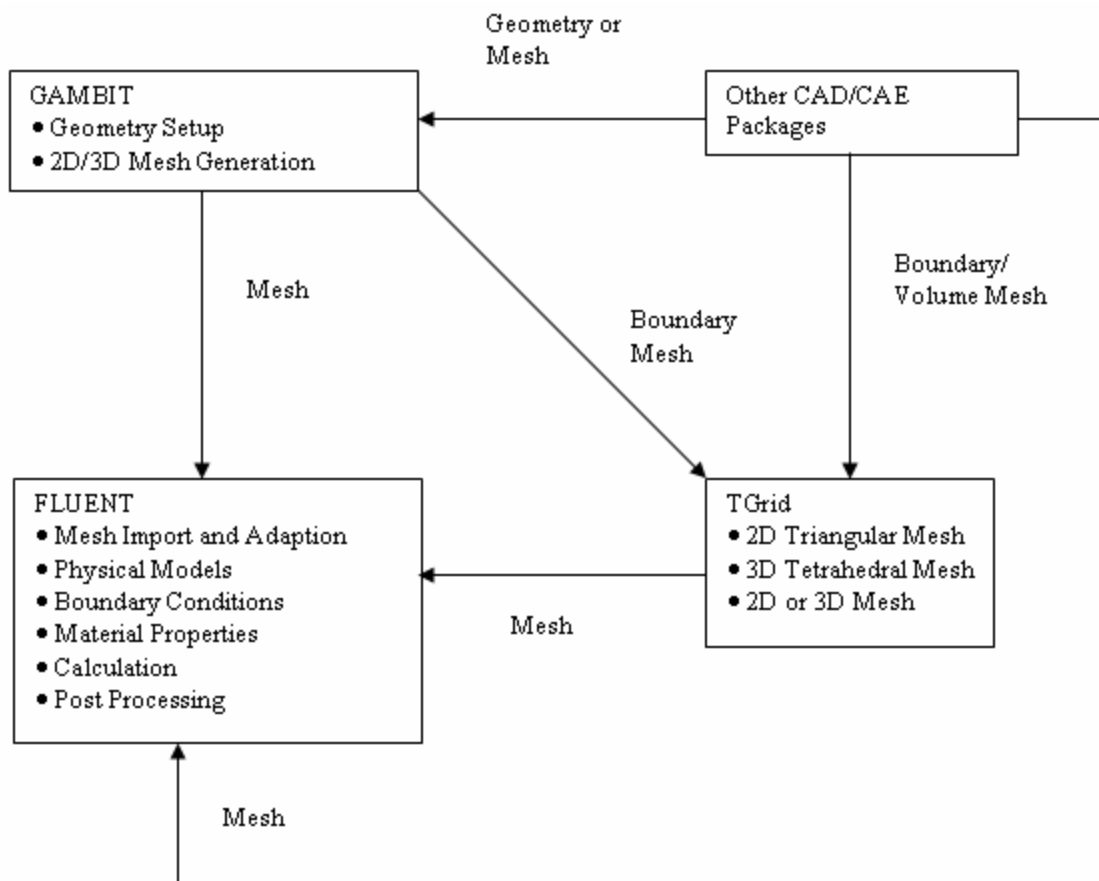


Figure 2.10 Basic Structure of FLUENT Program [21]

2.8.4. Modeling Capabilities. FLUENT has a wide range of modeling capabilities and can handle laminar and turbulent flows as well as single, multiphase, and discrete phase problems. These can be either steady or unsteady state. FLUENT can also treat complex systems that include transport phenomena, heat transfer, mass transfer, and chemical reactions. There are different multiphase models such as VOF, Mixture, Eulerian, and discrete phase models, which are described in detail in Section 2.9.6.

FLUENT can also be useful in modeling flow in moving or deforming zones [18]. The deforming zone may be defined by a single or multi-frame of reference. A single frame of reference is used when the whole domain is rotating and multiple frames of reference are used when some parts are rotating and some are stationary. In addition, the mesh movement may be either sliding or dynamic. A sliding mesh is used when there is

relative motion between two boundaries and a dynamic mesh is used when there is time dependent deformation or change of shape of the domain.

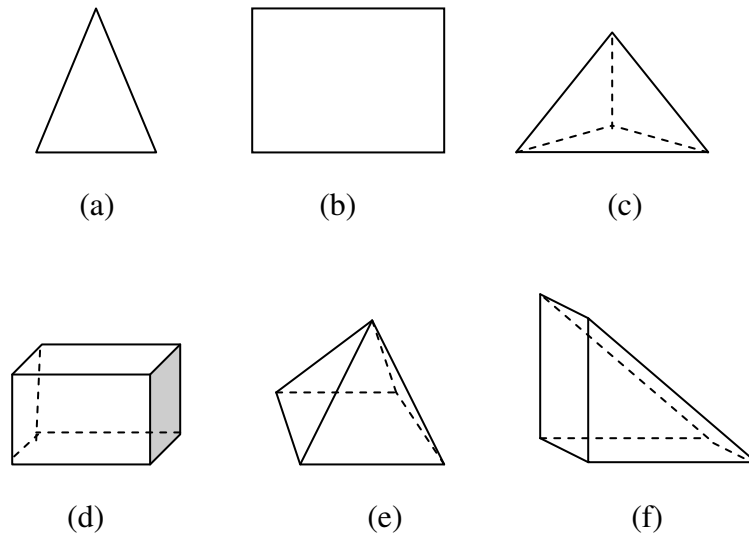


Figure 2.11 Different Mesh Elements, (a) Triangular, (b) Quadrilateral, (c) Tetrahedral, (d) Hexahedral, (e) Pyramid, (f) Wedge

2.8.5. Boundary Conditions. Boundary conditions are critical in solving a problem as they specify the proper parameters of the problem. Several boundary conditions can be specified in FLUENT for any given problem [18]. They are listed below.

- The boundary conditions at the inlets and exits may be specified by magnitude of velocity and pressure or mass flow rates. Other parameters such as phase volume fraction and species mass fraction can also be given as inputs for the corresponding models. The pressure outlet boundary condition is specified on the sides which are open to the atmosphere or to the outlets at which the pressure is specified. The gauge pressure can be set at the surface

- Wall boundary conditions are used for sides bounding solid and fluid zones. The wall may be of a no-slip condition at which the velocity components can be specified or the slip condition can be indicated by specifying the shear.
- The different internal zones are fluid, solid, and porous zones and the different boundary conditions available for internal cell boundaries are interior, fan, radiator, and porous jump. These are explained in detail in FLUENT user's guide [18].

2.8.6. Multiphase Models. There are several multiphase models in FLUENT [18]: VOF, Mixture, Eulerian, and discrete phase models. The VOF method is used for non-interpenetrating, stratified or free-surface flows. Both Mixture and Eulerian models are used for bubbly or particle flows where the particle volume fraction is less than 10%. For systems having more than 10% particle volume fraction, the discrete phase model is used.

VOF is the most commonly used method for two or more immiscible fluids and is used in this project. The VOF model can be coupled with other models such as species transport to account for mass transfer and phase change. A single continuity equation is solved for all the phases (Equation 2.13), and also includes a volume fraction term [18].

$$\frac{1}{\alpha_q} \left[\frac{\partial}{\partial t} (\alpha_q \rho_q) + \nabla \cdot (\alpha_q \rho_q \vec{v}_q) \right] = S \alpha_q + \sum_{p=1}^n (m_{pq} - m_{qp}) \quad 2.13$$

where α_q , ρ_q , and \vec{v}_q are the volume fraction, density, and velocity of the q^{th} phase, S is the source term, m_{pq} is the mass transfer rate from the p^{th} phase to q^{th} phase, and m_{qp} is the mass transfer rate from q^{th} phase to p^{th} phase. This equation also takes into account phase interactions, such as mass transfer and surface tension. Each cell is considered to be filled with all the phases. If there is only a single phase in a particular cell, its volume fraction is equal to one and the volume fractions of the other phases are zero. The sum of the volume fractions of all phases in a cell is 1.

$$\sum_{q=1}^n \alpha_q = 1 \quad 2.14$$

The momentum and energy equations are also shared among the phases where the equations are modified to include the volume fraction ‘ α ’ [18].

$$\frac{\partial}{\partial t}(\rho \vec{v}) + \nabla \cdot (\rho \vec{v} \vec{v}) = -\nabla p + \nabla \cdot [\mu (\nabla \vec{v} + \vec{v} \nabla^T)] + \rho \vec{g} + \vec{F} \quad 2.15$$

$$\frac{\partial}{\partial t}(\rho E) + \nabla \cdot (\vec{v}(\rho E + p)) = \nabla \cdot (k \nabla T) + S_h \quad 2.16$$

where \vec{v} is the overall velocity vector, p is the pressure, \vec{g} is the acceleration due to gravity, \vec{F} is the force vector, E is the total energy, k is the thermal conductivity, S_h is the source term, and ∇T is the temperature gradient.

The introduction of ‘ α ’ comes in the calculation of the properties of the mixture, which are calculated based on the properties of the phases and their volume fractions. The formula for calculating density is given below.

$$\rho = \sum \alpha_q \rho_q \quad 2.17$$

Similarly, the other properties in the governing equations, such as viscosity, are also calculated. Equations for other models such as turbulence are solved in a similar fashion.

Four schemes to calculate the fluxes for interface interpolation are geometric reconstruction, donor-acceptor, Euler explicit, and implicit schemes. The first two schemes use the standard interpolation schemes of FLUENT when the cell is filled with only one phase. If the cell includes an interface, a different method for each scheme is used to calculate the fluxes. The geometric reconstruction method uses a piecewise linear technique near the interface. A donor-acceptor method is used for the donor-acceptor scheme where one cell is considered as a donor for the fluid and another cell as the acceptor for that fluid. These methods are described in detail in the FLUENT manual [18]. The Euler explicit and implicit methods use standard interpolation techniques where values are updated based on the previous and current time steps, respectively. The geometric reconstruction scheme is the most commonly used as the tracking of the interface is more accurate.

2.8.7. Dynamic Mesh Motion. FLUENT also has the capability of solving problems with moving zones or boundaries. The dynamic mesh model is used if the shape of the domain is changing with time; examples include the falling of a solid body

or a moving car. The motion of the corresponding boundary can either be indicated from the boundary values or from a UDF. This is done by giving the linear or angular velocities directly or specifying them using a UDF which is described in the next section. For example, a UDF may be used for the motion of a wall after a certain amount of time. The six degrees of freedom model (6DOF) is used to update the position of the domain based on the force balances at a particular time step [18]. All these methods solve the dynamic mesh equation and update the position of the new mesh based on updating methods such as smoothing, layering, or re-meshing. The dynamic mesh conservation equation is given below [18]:

$$\frac{d}{dt} \int_V \rho \phi dV + \int_{\partial V} \rho \phi (\vec{u} - \vec{u}_g) d\vec{A} = \int_{\partial V} \Gamma \nabla \phi d\vec{A} + \int_V S_\phi dV \quad 2.18$$

where ϕ represents any scalar quantity over which the conservation equation is solved.

2.8.8. User Defined Functions. The standard FLUENT interface may not meet the requirements of all users. User defined functions are specific programs written by the user in the language C, and can be incorporated into FLUENT through a compiler or interpreter. There are specific macros which can be used to define specific conditions that access the variables from the FLUENT solver. Some UDF's may be either interpreted or compiled, while some can only be compiled depending on the macros used in the UDF. When a UDF is interpreted, each line of the program is translated into machine language and executed before going to the next line, whereas in compilation the whole program is translated at once. The UDF's may return a value or may be void. The void UDF's are used to modify a variable or to write a case or data file. There are also specific UDF's to simply write a case or data file. Once the UDF has been compiled it can be viewed in the pull-down menus of FLUENT, depending on the macros. For example, if the UDF is written to define the boundary condition at a particular wall, the UDF will be seen in the boundary conditions panel. Specific UDF's have specific calling sequences in FLUENT. These sequences vary from solver to solver and are described in the FLUENT manual. There are also some limitations to the UDF's as some of the variables cannot be accessed by the macros.

3. EXPERIMENTAL AND SIMULATION PROCEDURE

3.1. CONTACT PLANARIZATION PROCESS

The contact planarization process carried out at Brewer Science Inc. consists of a photoresist (S1818TM) coated on a Si substrate layer. The geometry of the layers before and after solvent evaporation is shown in Figure 3.1. The substrate surface has surface features as shown in Figure 3.1a. S1818 is then spin-coated onto its surface. The height of each feature is approximately 10 μm and the photoresist layer is 1.5-2 μm thick above the features. S1818 (a positive photoresist) mainly contains a solvent (propylene glycol monomethyl ether acetate, PGMEA), resin, and a photoactive compound.

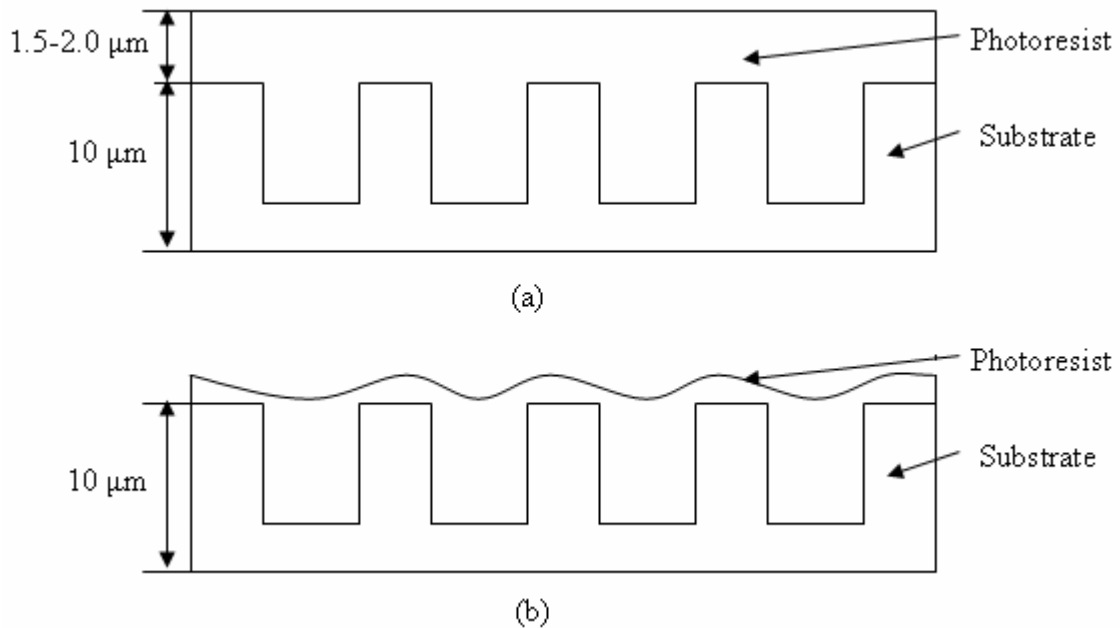


Figure 3.1 Photoresist Surface, (a) Before Solvent Evaporation, (b) After Solvent Evaporation

The purpose of the solvent is to make the fluid thinner and to make the deposition easier. After the photoresist is coated, the solvent is evaporated by a soft bake process at

a temperature of 115°C until the surface is no longer tacky. As the solvent is evaporated, the viscosity of the S1818 layer increases. The solvent allows the photoresist to flow at higher temperatures, which changes the shape of the surface. The photoresist layer also conforms to the topography of the layer below. A wavy surface (Figure 3.1b) is produced as a result of these phenomena. This is explained in detail in Section 1.2.4.

The process of wafer planarization is needed to planarize the photoresist surface. An optically flat surface, called a planarizing plate, is pressed against the surface of the photoresist to make it flat (Figure 3.2). This process is explained in Section 1.2.5.3.

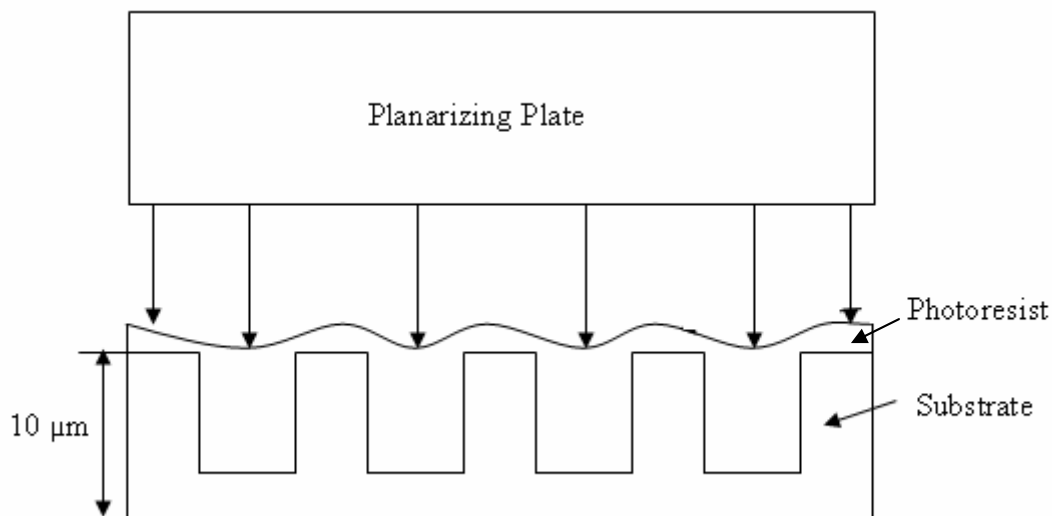


Figure 3.2 Contact Planarization

3.2. VISCOSITY EXPERIMENTS

The material properties of S1818 were needed to model contact planarization in FLUENT. Experimental measurements of viscosity values of S1818 at various solvent percentages were used to evolve a viscosity-solvent fraction relationship to model the behavior of the photoresist as the solvent evaporates. The viscosity of the photoresist was measured using a Brookfield cone and plate viscometer.

3.2.1. Apparatus for Viscosity Testing. The Brookfield cone and plate viscometer consists of a plate and several cones. Each cone has a specific range of viscosity measurement. The viscometer may be either dial, digital, or programmable; this work utilized a programmable type viscometer. The first two work on the same principle, but differ in the display of the viscosity reading. In dial and digital viscometers, shear rate or speed are specified and the viscosity is noted from the dial or the LCD display, respectively. In programmable viscometers, the viscometer is controlled by use of a software program. CAPCALC[®], an application software (Brookfield Engineering) was used to control the viscometer. The testing can be done either for a specific value of shear rate or speed or for a range of shear rates or speeds by using a built-in function in CAPCALC. First, the sample was placed on the plate and the cone was brought down to touch the sample as shown in Figure 3.3. The second step was to start the program and measure the viscosity for the specific values of shear rate or speed.

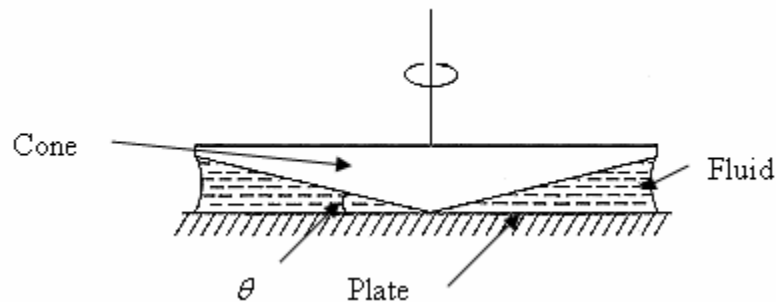


Figure 3.3 Cone and Plate with the Testing Fluid [22]

The viscosity, shear stress, and shear rates were calculated by the following formulas [37]:

Viscosity ‘ η ’:

$$\eta = \frac{\tau}{\dot{\gamma}} \quad 3.1$$

Shear Stress ‘ τ ’:

$$\tau = \frac{M}{\frac{2}{3}\pi r^3} \quad 3.2$$

Shear Rate ‘ $\dot{\gamma}$ ’:

$$\dot{\gamma} = \frac{\omega}{\sin \theta} \quad 3.3$$

where ω is the angular velocity of the cone, θ is the angle of the cone as shown in the figure, M is the torque input by the viscometer, and r is the radius of the cone.

The main advantage of this viscometer over other types of viscometers is that it requires extremely small amounts of sample (0.5 – 2 mL). Temperature control is very easy, which can be advantageous for testing temperature-dependent viscosity. A constant temperature bath, placed in a jacketed device below the plate, is used to control the temperature. The operating and set temperatures can be monitored in the computer through the CAPCALC software.

3.2.2. Experimental Procedure. The first step in sample preparation was to find the amount of solvent present in the S1818 sample given by Brewer Science. A known weight of this sample was taken in a beaker and kept in a vacuum chamber to which a gauge pressure of -30 inHg was applied. As S1818 is a photoresist and polymerizes on exposure to light, the vacuum chamber and the beaker were covered with aluminum foil to prevent exposure to light. The weight of the sample was measured at different time intervals, and the percentage of sample evaporated during that time interval was calculated. The solvent was considered to be completely evaporated when the difference between two consecutive weight readings was negligible. Two runs were carried out to find the solvent percentage in the original sample, and the viscosity of the original sample was measured by the procedure explained below. The experimental setup of the vacuum pump and chamber is shown in Figure 3.4.

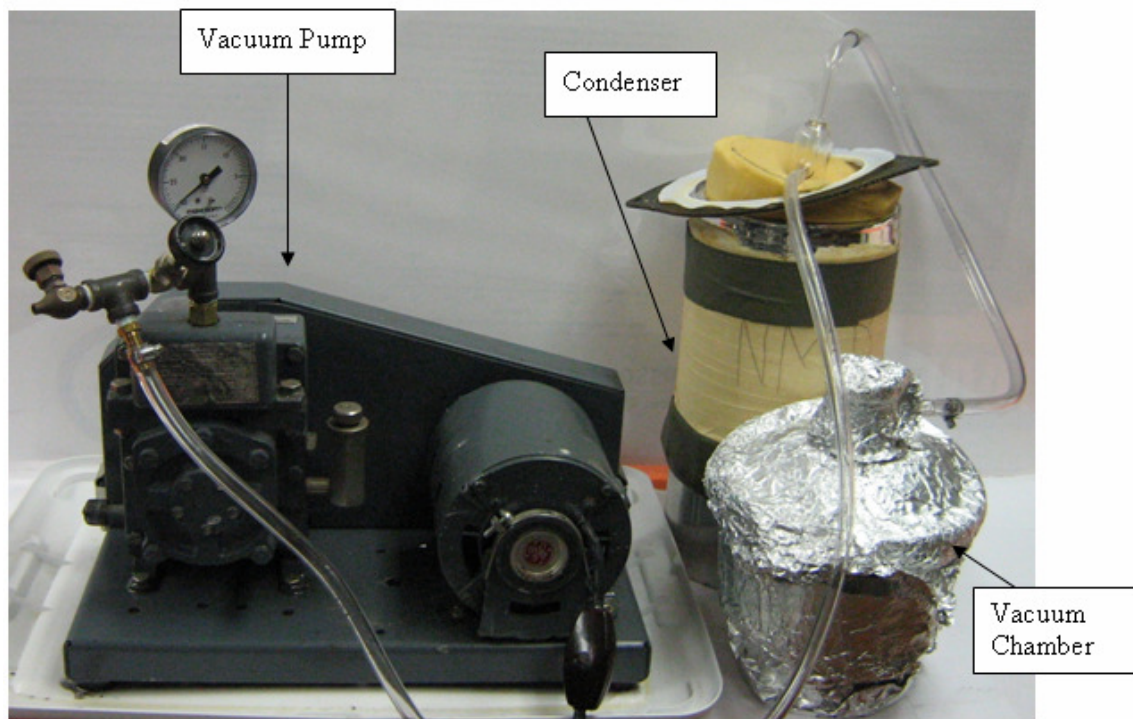


Figure 3.4 Vacuum Pump Setup

The viscometer was first calibrated with a calibrating fluid whose viscosity was known at room temperature. The calibration was done every day before starting the experiment and each time the cone was changed. After calibration, the sample was placed on the plate, the cone was brought down to touch the sample, and the program was started. The viscometer was controlled by the computer and the values were recorded for each run. The viscosity of the sample was measured and reported by the program at speeds ranging from 50 through 500 RPM, in increments of 25 RPM. The results were viewed, analyzed, and stored for future use, and were also exported to a Microsoft Excel file. A power law model was fitted to the data to obtain the values of the consistency index, k , and flow index, n , where k and n are defined by the following relation [37]:

$$\tau = k \left(\dot{\gamma} \right)^n \quad 3.4$$

The next step was to study the viscosity of S1818 with different solvent percentages. Samples containing different solvent percentages were prepared. The same sample preparation steps were used, but evaporation was carried only until the point where the sample contained the required percentage of solvent. Samples with 31, 25, 21, and 10% solvent were prepared and their viscosities were measured.

3.3. CFD PROCEDURE

The mathematical analysis of this problem involves solving the continuity, momentum, volume fraction, and mass transfer equations. There are two sets of flow equations in CFD, one for viscous flow and another for inviscid flow. As this problem involves incompressible flow and viscous effects are important, the following set of equations must be solved (Appendix A). The momentum equations (3.6-3.8) shown below include the viscous terms. The volume fraction equation also has to be solved to track the interface after the mass transfer process.

Continuity equation [19]:

$$\frac{\partial \rho}{\partial t} + \nabla \cdot (\rho V) = 0 \quad 3.5$$

x-momentum equation [19]:

$$\frac{\partial(\rho u)}{\partial t} + \nabla \cdot (\rho u V) = -\frac{\partial p}{\partial x} + \frac{\partial \tau_{xx}}{\partial x} + \frac{\partial \tau_{yx}}{\partial y} + \frac{\partial \tau_{zx}}{\partial z} + \rho f_x \quad 3.6$$

y-momentum equation [19]:

$$\frac{\partial(\rho v)}{\partial t} + \nabla \cdot (\rho v V) = -\frac{\partial p}{\partial y} + \frac{\partial \tau_{xy}}{\partial x} + \frac{\partial \tau_{yy}}{\partial y} + \frac{\partial \tau_{zy}}{\partial z} + \rho f_y \quad 3.7$$

z-momentum equation [19]:

$$\frac{\partial(\rho w)}{\partial t} + \nabla \cdot (\rho w V) = -\frac{\partial p}{\partial z} + \frac{\partial \tau_{xz}}{\partial x} + \frac{\partial \tau_{yz}}{\partial y} + \frac{\partial \tau_{zz}}{\partial z} + \rho f_z \quad 3.8$$

Volume fraction equation [18]:

$$\frac{1}{\alpha_q} \left[\frac{\partial}{\partial t} (\alpha_q \rho_q) + \nabla \cdot (\alpha_q \rho_q \vec{v}_q) \right] = S \alpha_q + \sum_{p=1}^n (m_{pq} - m_{qp}) \quad 3.9$$

The solution for this problem is obtained by solving the above equations. First, the continuity equation is solved and then the momentum equations are solved to get the velocity field. As the momentum equations contain non-linear or coupled terms ($\rho uV, \rho vV, \rho wV$), the velocity field can be obtained by solving the above set of equations, which is much more difficult than solving a single equation. As this process is temperature dependent, the energy equation must also be solved (Appendix A). Equation 3.8 must be solved to obtain the shape of the interface between the phases. This equation contains a source term, S , and the interaction term, \dot{m} , which includes the mass transfer between the phases. The whole set of equations must be solved at each time step as it is an unsteady process, which requires even more computational effort. An analytical solution is impossible and iterative methods are needed to solve the equations, which can be done using software such as FLUENT.

3.4. MODELING SETUP FOR EVAPORATION PROCESS

The mesh of the computational domain for the evaporation process was created in the preprocessor, GAMBIT 2.2.30. For ease of design, the geometry of the mesh was created at 10^6 times the original dimensions and then scaled down in FLUENT. A zone of air above the required geometry was also considered to be a part of the computational domain as the evaporation process involves the interaction between air and the photoresist. The geometry of the computational domain is shown in Figure 3.5. As shown in the figure, the zone above is air and the one below is the photoresist. After creation of the geometry, the boundary types were specified. All the edges were defined as walls except the edge between air and fluid zones, which was defined as an internal zone.

The meshing of the computational domain was then done by using a constant interval size option. An interval size of 0.1 was used for all the edges. The mesh of the computational domain is shown in Figure 3.6. After the mesh was generated, it was examined for the presence of any distorted elements, which may be obtained because of improper interval sizes for different edges or by not choosing the proper mesh type for a given geometry. A good mesh should not contain any distorted elements as the CFD

analysis can be used only for regular element shapes. The mesh was then exported to FLUENT.

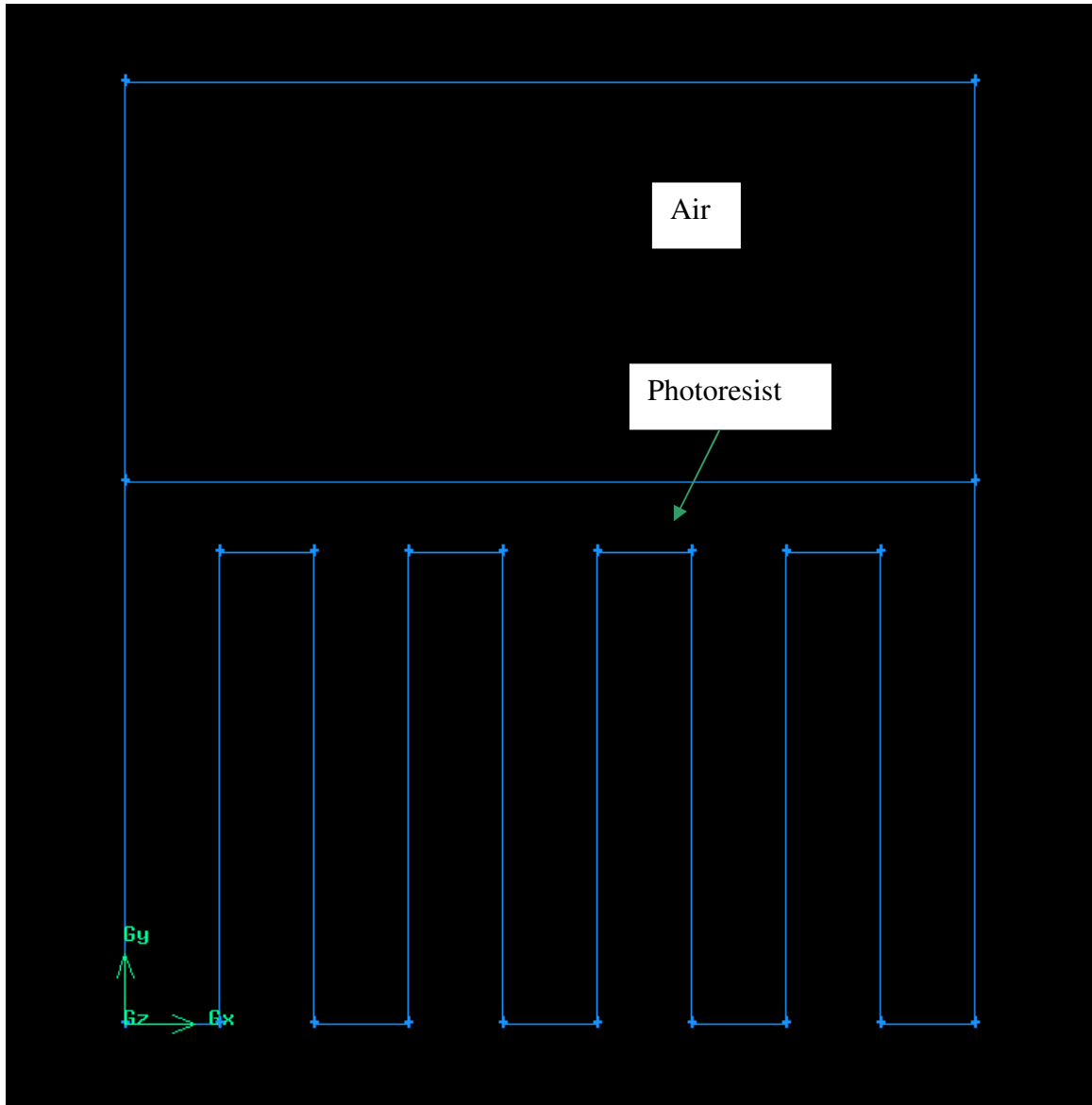


Figure 3.5 Geometry of the Computational Domain for the Evaporation Process

The exported mesh was opened in FLUENT 6.3.26 and a grid check was performed to check for negative volumes, which indicate improper connectivity between

the cells. The grid is not correct if it contains any cells with negative volumes as the discretization would result in unphysical results [18]. The checked grid was then scaled down to the required dimensions. The required model setup in FLUENT is shown in Table 3-1. The first column shows the menu of the FLUENT interface where the models are selected and the second column shows which models were chosen for the evaporation process. In FLUENT there are some default models and values. The third column shows any changes to these default values.

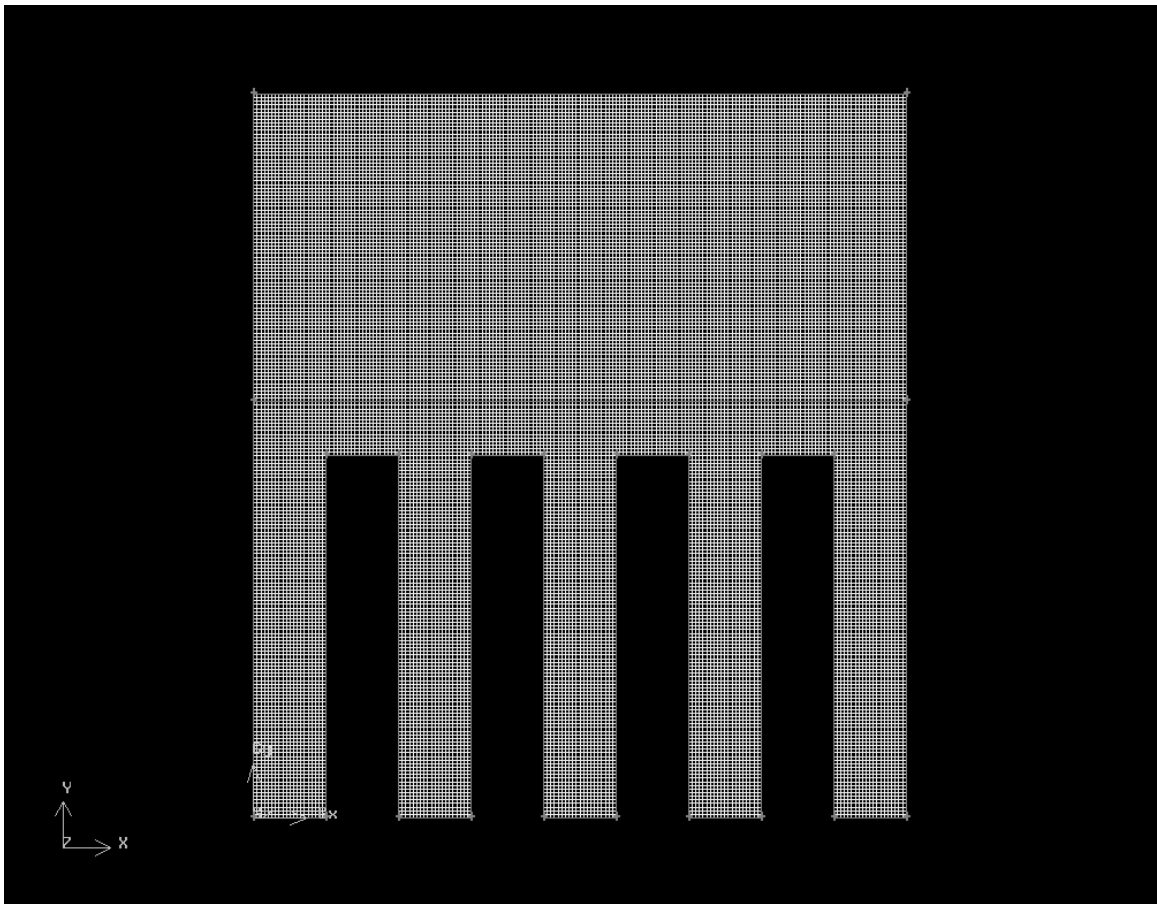


Figure 3.6 Computational Domain Mesh for the Evaporation Process

Table 3-1: Model Properties of the Evaporation Simulation

Menu Panel	Models Selected	Models Unselected
1) Define→Models→Solver Selecting unsteady state condition	Unsteady state Node based formulation	None
2) Define→Models→Multiphase Selecting a multiphase model	VOF with 2 phases Implicit body force	None
3) Define→Models→Energy Selecting to solve the energy equation as the operating temperature is 118°C	Energy equation	None
4) Define→Models→Species→Transport and Reaction Selecting transport of species model	Species transport	None
5) Define→Phases Defining the phases	Primary phase- air-solvent vapor Secondary phase- S1818 with solvent	None
6) Define→Operating Conditions Defining the operating conditions	Gravity = -9.81 m/s ² in the y-direction Reference pressure location (x, y): (0, 1.50e-5) Operating temperature : 388.15 K Specified operating density	None
7) Define→User Defined→Functions→Interpreted Connecting the UDF to FLUENT	UDF shown in Appendix B is selected and interpreted	None
8) Define→User Defined→Function Hooks Connecting specific parts of UDF to specific panels in FLUENT	The corresponding part of the UDF is selected in adjust panel	None
9) Define→User Defined→Scalars Defining UDS to a particular variable which is not built in FLUENT	Number of user defined scalars (UDS) = 1 Phase is primary phase	None
10) Define→User Defined→Memory Allocating the memory location to the UDS	Number of user defined memory locations = 1	None
11) Adapt→Region Marking the region for one of the phases	Input coordinates: (x, y) Minimum: (0, 0) Maximum: (1.80e-5, 1.15e-5) Adapted and marked	None
12) Solve→Monitors→Residual Plotting the residuals	Plot residuals selected	None
13) Solve→Initialize Initializing	Temperature = 388.15 K	None
14) Solve→Initialize→Patch Initializing	Phase – S1818 Volume fraction = 1 Solvent mass fraction = 0.2	None

The material properties were defined only after defining the models (after Step 4 in Table 3-1) as the mixture type of material is activated only after choosing the species transport model. A volume weighted mixing law was chosen to calculate the density of the materials. The viscosities of the gaseous and liquid phases were $1.78\text{e-}5$ kg/m-s and $1.10\text{e-}3$ kg/m-s, respectively. A constant viscosity for S1818 was used for ease of convergence. The viscosity of S1818 after evaporation should be changed to the viscosity of S1818 at zero percentage solvent before starting the plate motion.

The evaporation was to be based on a VOF gradient, so a UDF was written to account for this (Appendix B). The adapted region for Step 11 is shown in Figure 3.7. The shaded zone shows the marked region, which was later patched. After initialization, an animation file was started to record the volume fraction of the secondary phase at each time step. The surface integral of the solvent in S1818 was also monitored to check for the percentage of the solvent at any time interval. A time step of size 0.01 s was used. The simulation was iterated for three time steps and then the mass transfer part of the UDF was hooked in the phase interaction panel. After that, it was run for two more time steps to calculate the VOF gradient. The contours of the user defined memory variable were observed, the value of the VOF gradient was changed in the UDF, and the UDF was interpreted.

3.5. MODELING SETUP FOR THE PLATE MOTION

The step after the evaporation process involves the plate motion to planarize the surface of the S1818. Dynamic mesh motion was used in FLUENT to model the plate motion. Since the mesh was not deforming with time and only the cells on the sides of the plate were expanding or contracting, a sliding mesh model was used. In a sliding mesh model, a moving edge slides along one or two edges. The mesh generation steps were almost the same as those of the evaporation process. Duplicate edges were required for the creation of sliding edges, i.e. two edges must overlap to form the sliding edge each corresponding to different faces. The mesh for the plate motion is shown in Figure 3.8.

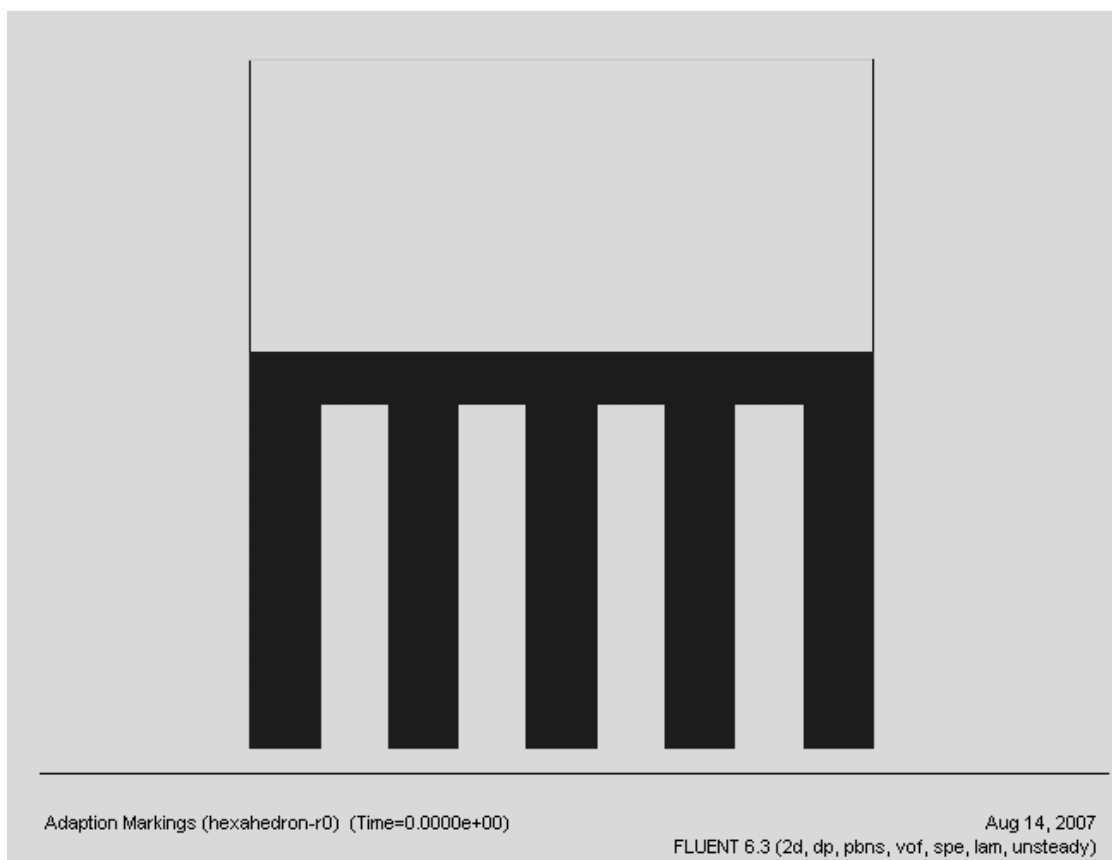


Figure 3.7 Adapted Region for the Secondary Phase

After exporting the mesh to FLUENT, the grid interfaces were defined in the Define→Grid Interfaces panel. The same steps were followed for scaling and grid checking. The models used in this step are described in Table 3-2. All other conditions that are not described here are the same as in the evaporation process.

The dynamic mesh simulation was run after obtaining the wavy pattern in the evaporation process. The simulation becomes more complex when both species transport and dynamic mesh are enabled. To make the simulation simpler, the dynamic mesh simulation was performed without the evaporation process. The surface was adapted to resemble the wavy pattern resulting from the evaporation process to check for the interaction between the plate and the fluid. For simplicity, only one hump was included instead of many humps. Brewer Science continues the evaporation process until the solvent is no longer tacky, and since it was observed from experiments that S1818 was

not tacky at a viscosity of 22 Pa·s, this was chosen as the target viscosity for the simulations. The adapted zone for the plate motion portion shown in Figure 3.9 was slightly different from the one used during evaporation.

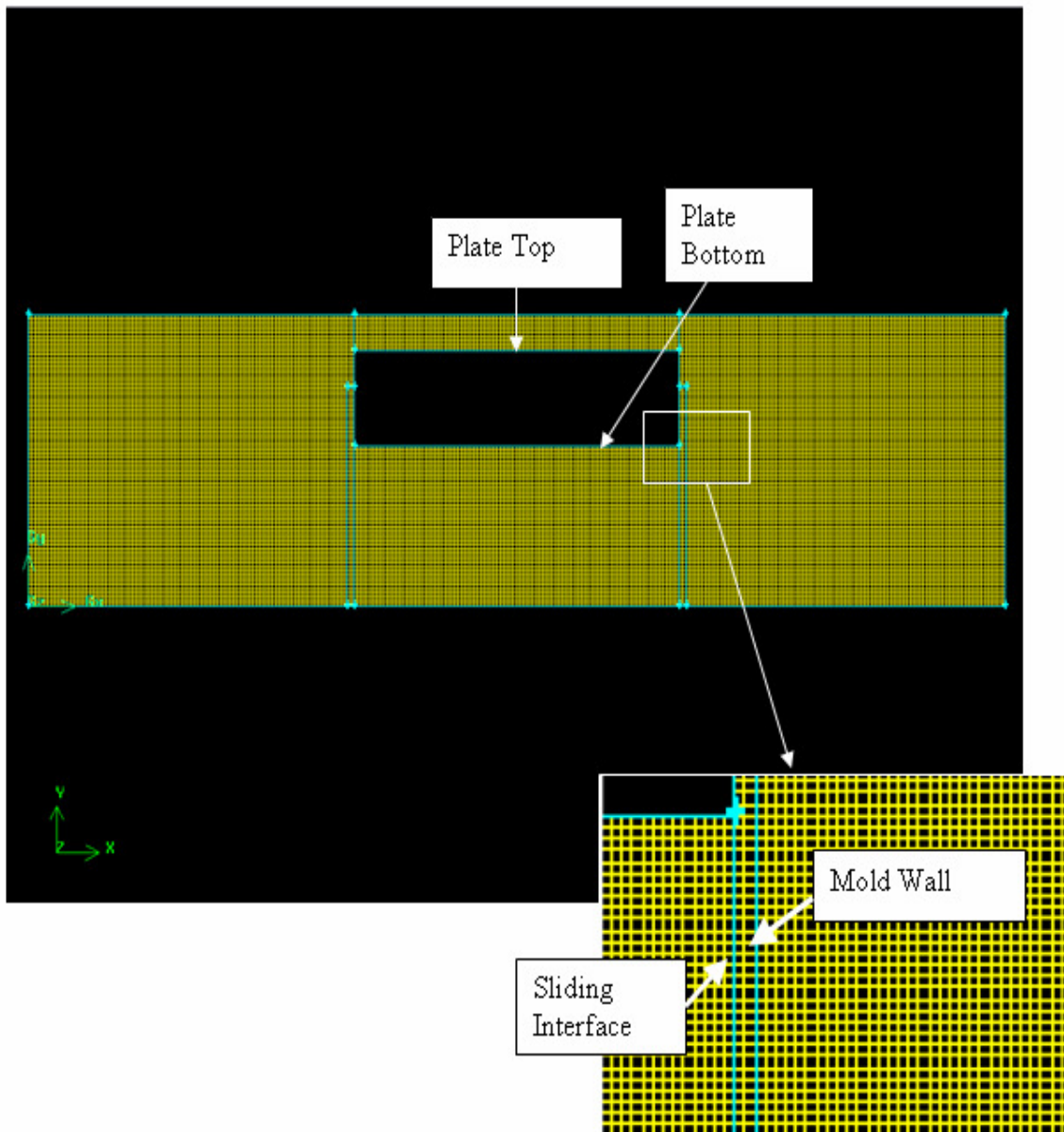


Figure 3.8 Mesh for the Plate Motion Showing the Different Boundary Types

Table 3-2: Model Properties of the Plate Motion Simulation

Menu Panel	Models Selected	Models Unselected
1) Define→Models→Solver	Cell based formulation	Node based formulation
2) Define→Models→Energy	None	Energy equation
3) Define→Models→Species→Transport and Reaction	None	Species transport
4) Define→Materials	Copy water from FLUENT database	None
5) Define→Phases	Primary phase – air Secondary phase – water	None
6) Define→User Defined→Functions→Compiled	UDF is compiled	None
7) Define→Dynamic Mesh→Parameters	Dynamic mesh Layering	Smoothing
8) Define→Dynamic Mesh→Zones	UDF based motion for plate bottom and plate top	None
9) Adapt→Region	Quad: (x, y) Minimum: (4.90e-6, 0) Maximum: (10.10e-6, 2.00e-6) Circle: (x, y) Center: (7.50e-6, 1.00e-6) Radius: 1.20e-6	None
10) Solve→Controls→Solution	Pressure velocity coupling: PRESTO Volume fraction discretization: Modified HRIC	None
11) Solve→Monitors→Residual	Plot residuals	None
12) Solve→Initialize→Patch	Secondary phase: volume fraction is 1	None

The contact planarization process requires the creation of a vacuum to prevent the recirculation of air when the plate is pressed against the fluid surface. The creation of a vacuum in a microscale geometry increases the Knudsen number when compared to the same value on the macroscale. The Knudsen number is defined by the following equation [18]:

$$Kn = \frac{\lambda}{L} \quad 3.10$$

where λ is the mean free path and L is the characteristic length of the system. The value of the Knudsen number must be less than 0.001 for CFD to be valid as it is a condition for the continuum regime to exist. As the geometry is on the microscale, the value of the

Knudsen number is much greater than 0.001 for any given mean free path, making it invalid for CFD analysis. To prevent recirculation, a source term is added to remove a volume of air which is equivalent to the volume displaced by the plate motion at each time step. A UDF was written to account for this, and is shown in the second part of Appendix B.



Adaption Markings (combination-r3)

Aug 14, 2007
FLUENT 6.3 (2d, dp, pbns, lam)

Figure 3.9 Adapted Region for the Plate Motion

4. RESULTS AND DISCUSSION

4.1. VISCOSITY MEASUREMENT

The experimental procedure explained in Section 3.2.2 was used to determine the mass percentage of solvent in the S1818 sample obtained from Brewer Science. The weight of the sample was measured at different time intervals and the mass percentage of sample evaporated was calculated. The percentage of sample evaporated at different time intervals for two runs is shown in Figure 4.1.

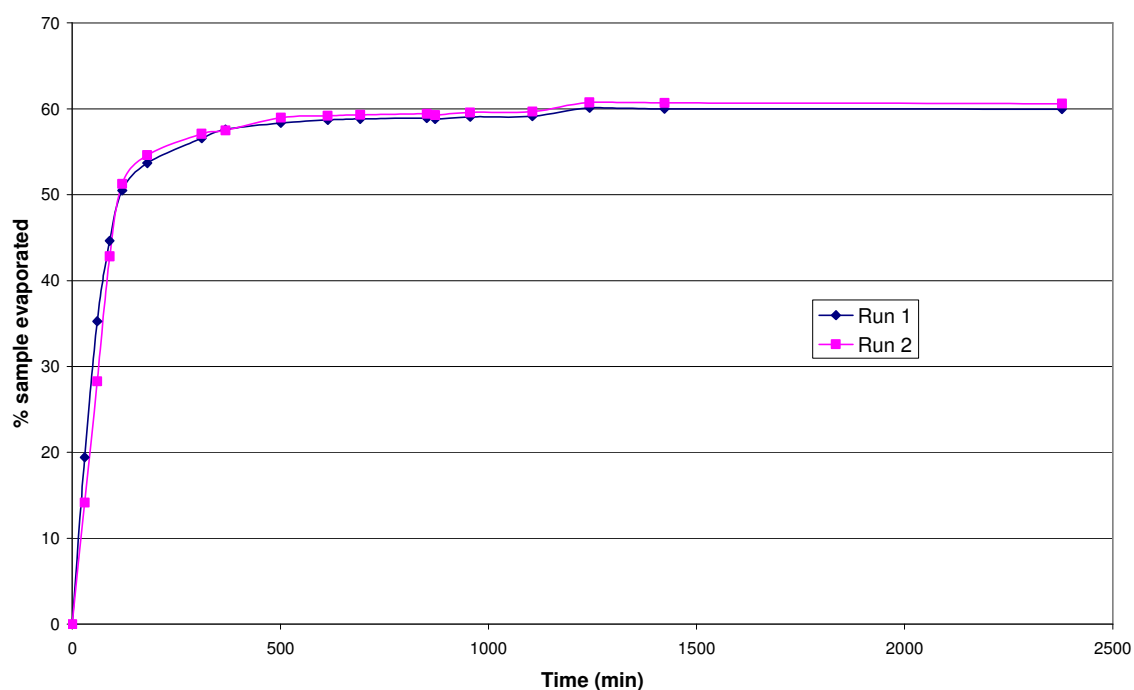


Figure 4.1 Percentage by Mass of Sample Evaporated

The rate of evaporation of solvent from the sample was found to be directly proportional to the amount of solvent present in the sample. As solvent evaporates, the rate of evaporation slows down and the difference between consecutive measurements of the sample weight decreases with time. When there remains a negligible difference

between two consecutive readings, a negligible quantity of solvent is assumed to remain in the sample. As the solvent is the only evaporating species in S1818, the final percentage of sample evaporated will be equal to the percentage of the solvent in S1818 initially. The above plot shows that there was an average of 60.3% solvent in the original given sample.

The viscosity of the sample with 60.3% solvent was measured and shear stress was plotted against shear rate on a logarithmic scale to determine whether the fluid is Newtonian or non-Newtonian. Five runs were carried out for the viscosity measurement of the sample. The plot from one of the runs is shown in Figure 4.2.

The power law is given by Equation 3.4. This equation can be rewritten by taking logarithms of both sides.

$$\log(\tau) = \log(k) + n(\log \dot{\gamma}) \quad 4.1$$

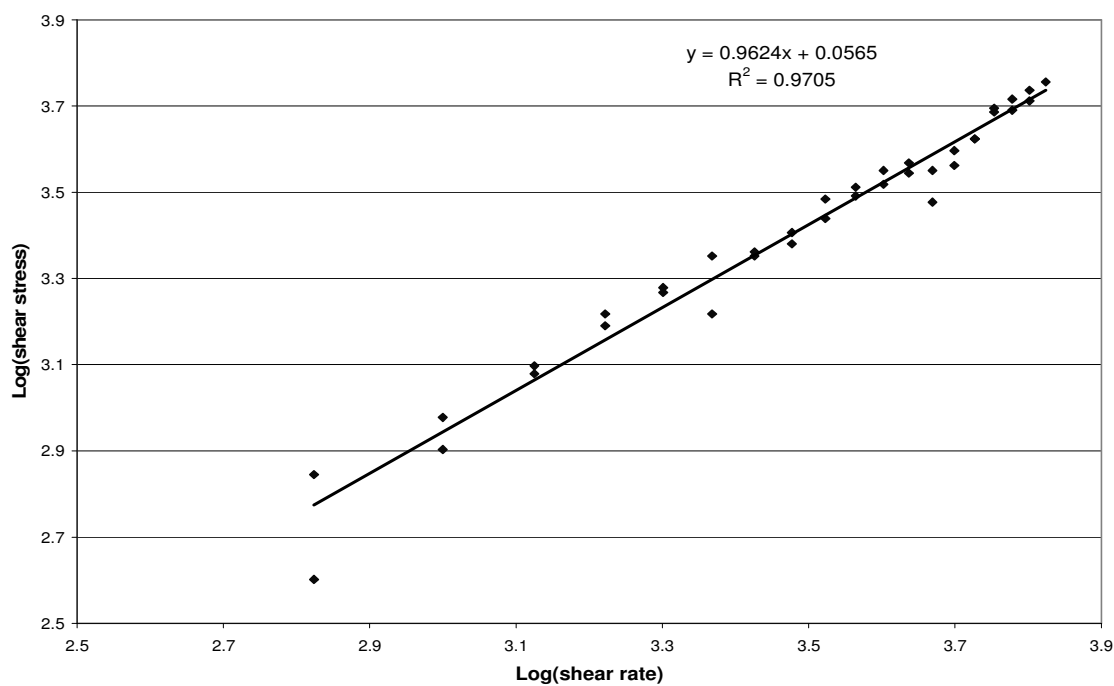


Figure 4.2 Power Law Plot for S1818 with 60% Solvent

Comparison of equation 4.1 to the equation in Figure 4.2 gives the value of the flow index, n . Table 4-1 shows the value of n for several runs, and an average value of 0.99 was obtained. Since this value is almost equal to 1, S1818 with 60.3% solvent can be considered as a Newtonian fluid.

Table 4-1: Flow Index Values for Different Runs of the Original Sample

Run Number	Flow Index 'n'
1	1.01
2	1.06
3	1.00
4	0.97
5	0.92

The samples with 31.5, 24.9, 21.9, and 11.2% solvent were prepared and their viscosities were measured. Plots similar to Figure 4.2 were generated and the values were noted. Three viscosity measurements were carried out for each sample. Table 4-2 shows the average flow index values for different percentages of solvent.

Table 4-2: Flow Index Values for S1818 with Different Solvent Percentages

Solvent Percentage	Flow Index 'n'
60.3	0.99 ± 0.08
31.5	0.98 ± 0.01
24.9	0.99 ± 0.01
21.9	0.97 ± 0.01
11.2	0.89 ± 0.28

It can be observed that as the solvent percentage decreases, S1818 acts almost Newtonian until the solvent percentage is 21.9 and then begins to behave as a non-Newtonian fluid, i.e. the value of n becomes less than 1. Since n decreases, the fluid appears to follow a shear-thinning behavior. This must be verified by measuring the viscosity of S1818 at several solvent percentages less than 21.9. Due to limitations of the apparatus, viscosity measurements of S1818 with solvent percentages lower than 11.2 could not be performed for this work. Viscosity measurements must be carried out to find the solvent percentage at which the non-Newtonian behavior starts.

The average viscosities of all the samples were plotted to obtain a relationship between solvent percentage and viscosity (Figure 4.3). It can be observed that the viscosity data follow a power relation, and the viscosity of the S1818 solution decreases with increasing solvent percentage as shown in the figure. This relationship can be used to specify the material properties of the evaporation simulation in FLUENT.

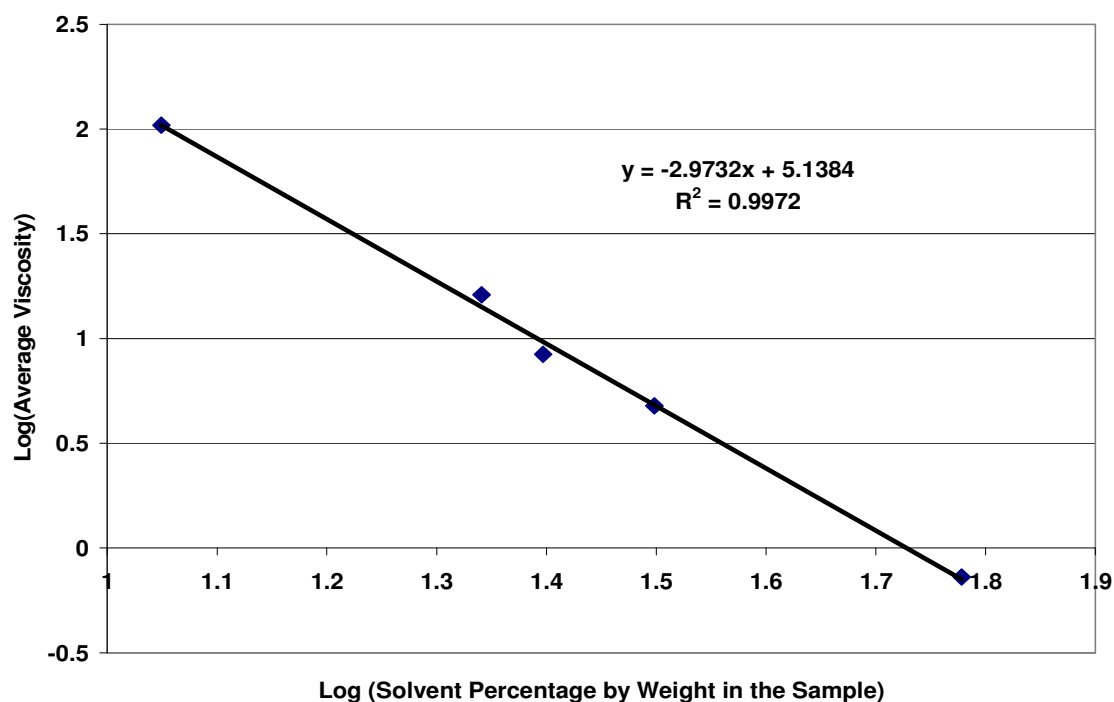


Figure 4.3 Relationship Between Average Viscosity and Solvent Percentage of S1818

4.2. EVAPORATION

The evaporation process was carried out until all the solvent evaporated. The S1818 and air phases before and after evaporation are shown in Figure 4.4. It is observed that a wavy surface appeared after evaporation due to shrinkage of the S1818 layer. As the layer shrinks, the zone above the trenches conforms to the shape of the trenches, causing depressions on the surface. On the other hand, the portions of the layer unsupported by a trench do not change their shape, leaving them elevated. The resultant of these elevations and depressions produces the wavy pattern shown in Figure 4.4b.

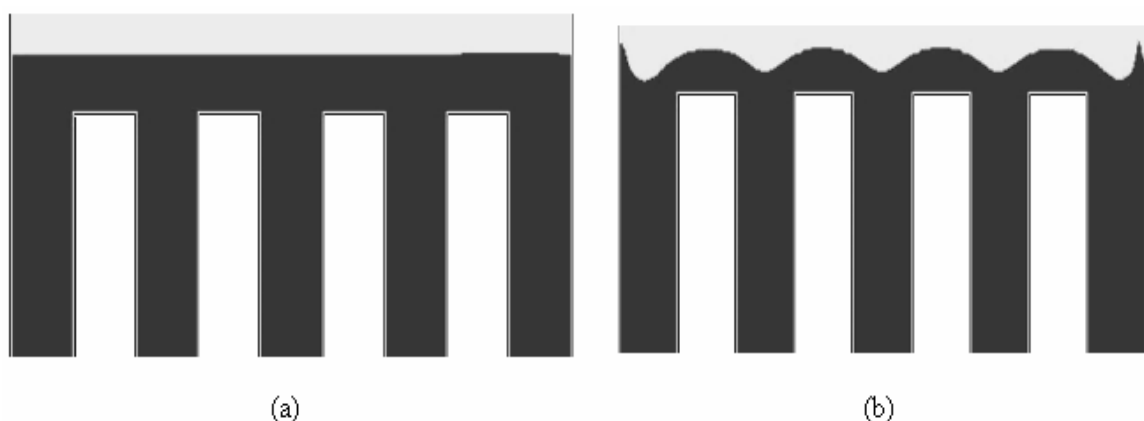


Figure 4.4 Phases - S1818 and Air – Evaporation , (a) Before Evaporation Process (0.06 s), (b) After Evaporation Process (0.15 s), (Black – S1818, Gray –Air)

4.3. DYNAMIC MESH MOTION

The dynamic mesh model for the plate motion was run for S1818. The surface of the S1818 layer became nearly flat and the plate stopped according to the conditions specified in the UDF. The contours of the S1818 phase before and after the planarizing process are shown in Figure 4.5. A slight rise in the liquid level in the gap between the mold wall and the interface is observed. This should not be observed at high viscosities. Further analysis is needed to investigate the reason for this effect. A different approach for modeling a vacuum, such as a molecular dynamics simulation, could explain this

effectively. Since the Knudsen number is higher for a vacuum than for systems at atmospheric pressure, statistical mechanics should be used.



Figure 4.5 Phases - S1818 and Air - Planarization, (a) Before Planarization (0 s), (b) After Planarization (1.50×10^{-5} s), (Black – S1818, Gray – Air, and White - Plate)

The plots for static pressure on the plate at different simulation times for a plate velocity of 0.01 m/s are shown in Figures 4.6 and 4.7. The data were split into two plots to facilitate analysis. Figure 4.5 shows the pressure data from 0 s to 8.00×10^{-6} s and Figure 4.6 shows the data from 1.00×10^{-5} s to 1.50×10^{-5} s. From the simulation it was observed that the plate stopped at 1.48×10^{-5} s. It can also be seen that the pressure on the plate increases as time proceeds and decreases after the plate stops. The highest pressure on the plate at 0.01 m/s is 150 MPa at 1.47×10^{-5} s, which is just before the plate stopping time. The reason for the shape of the pressure curve can be understood from the comparison plot shown in Figure 4.8.

A comparison between the pressure distribution along the plate and the shape of the interface is shown in Figure 4.8. Plots of the pressure and volume fraction are presented with a corresponding snapshot of the phase contour at three different time instances during the simulation (1.00×10^{-6} , 8.00×10^{-6} , and 1.30×10^{-5} s). The pressure exerted on the fluid by the plate is in the downward direction, and since the fluid has a resistance

to flow, a pressure acts on the plate in the upward direction. The pressure exerted on the plate by the S1818 is due to the dominant viscous forces.

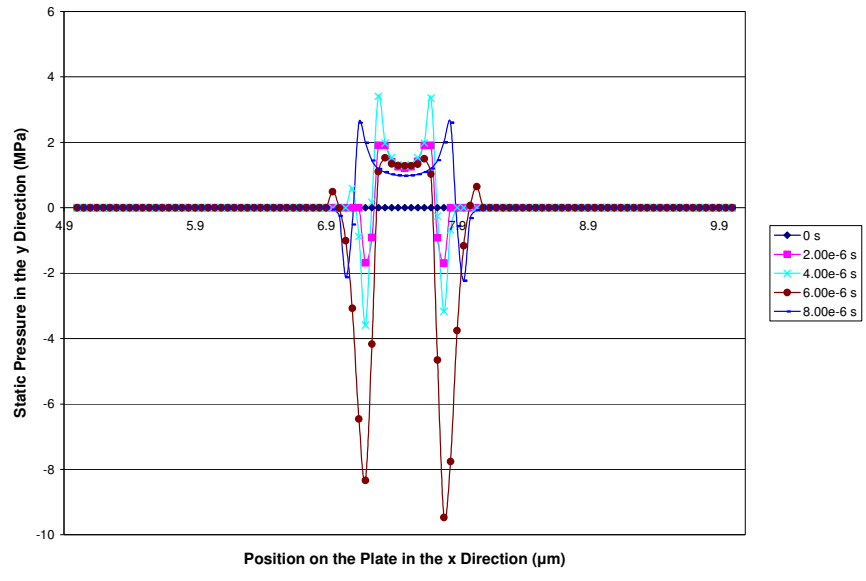


Figure 4.6 Static Pressure from 0 s to 8.00e-6 s for a Plate Velocity of 0.01 m/s

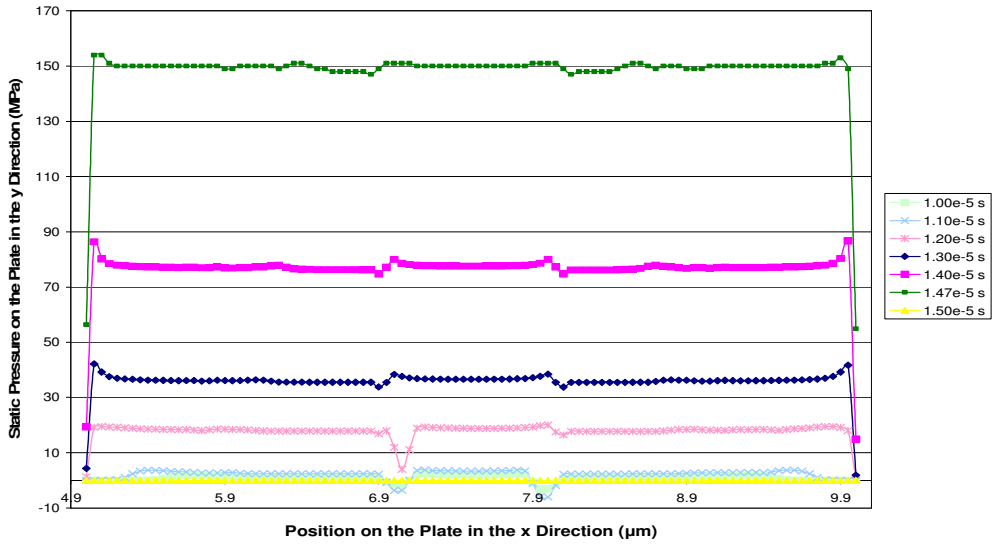
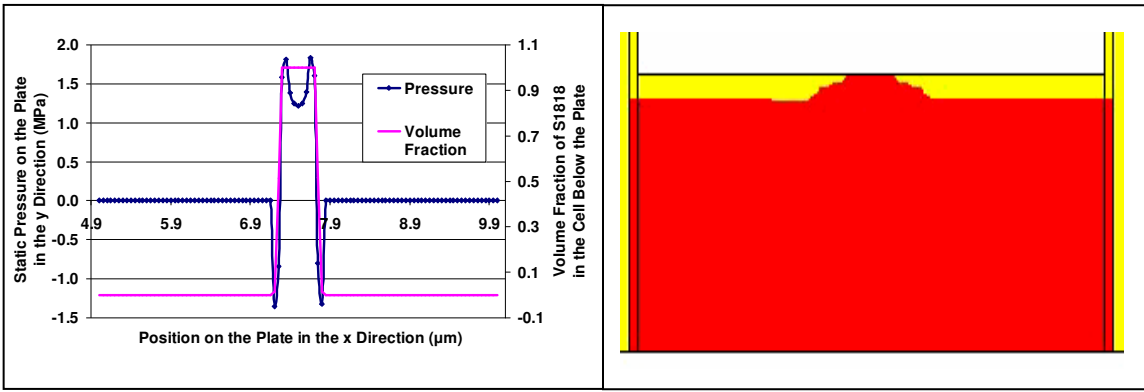
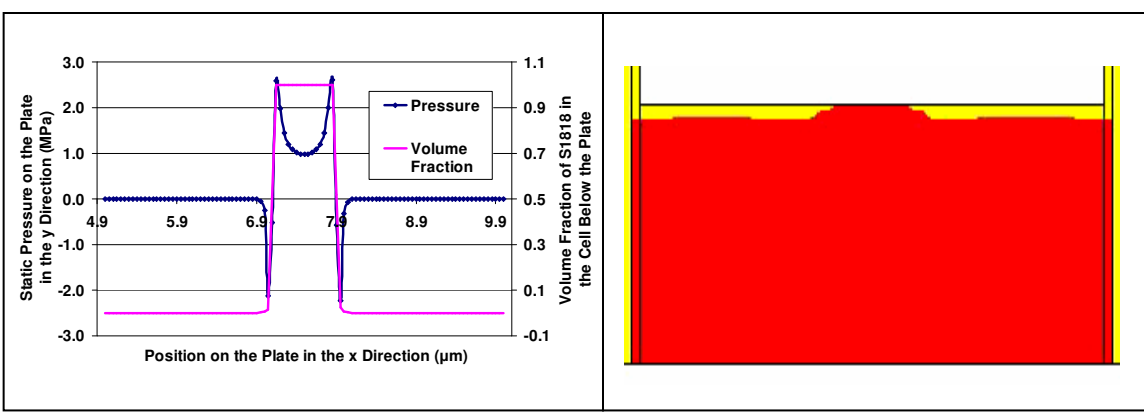


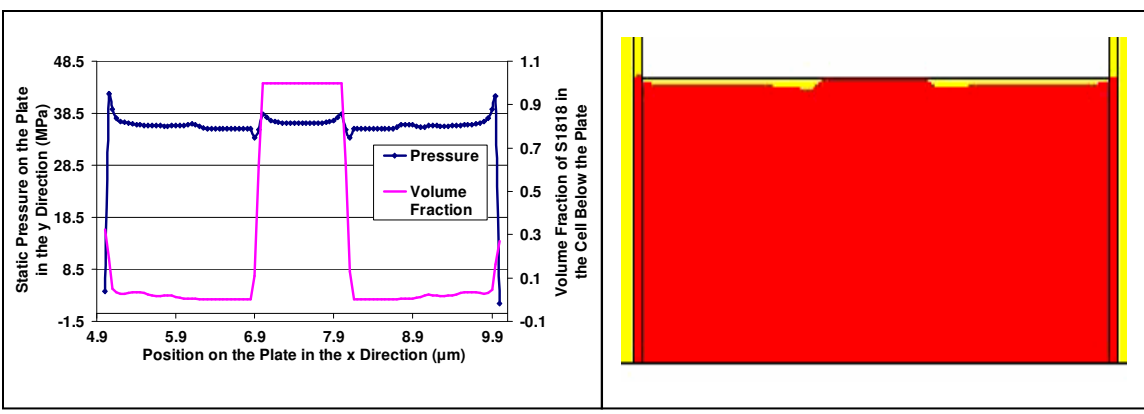
Figure 4.7 Static Pressure from 1.00e-5 s to 1.50e-5 s for a Plate Velocity of 0.01 m/s



(a)



(b)



(c)

Figure 4.8 Comparison of Pressure and Contour Plots at a Plate Velocity of 0.01 m/s, (a) Time = 1.00×10^{-6} s, (b) Time = 8.00×10^{-6} s, (c) Time = 1.30×10^{-5} s

As the plate touches the highest point of the fluid, the pressure exerted by the plate is felt first at that point, and as the plate continues to move downward, it exerts even more pressure on the surface of the fluid. At one point the resistance of the fluid is overcome by the pressure exerted by the plate and the fluid starts moving. This indicates the starting of the planarization process. The pressure at these points is lower than at the neighboring points where the fluid is still stagnant and has resistance to flow. At points on the plate surface where it is not touching the fluid, there is no pressure acting on the plate.

Dynamic mesh simulations were carried out for three different plate velocities (0.01 m/s, 0.005 m/s and 0.001 m/s) for a fluid viscosity of 22 Pa·s. The evaporation process at Brewer Science was continued until S1818 was not tacky. Since the fluid was not observed to be tacky at 22 Pa·s, this value was chosen for the simulation. The maximum pressure exerted on the plate at different simulation times was noted. Figure 4.9 shows the plot for maximum pressure at different simulation times for different plate velocities. The highest pressure on the plate for a viscosity of 22 Pa·s was observed for a plate velocity of 0.01 m/s and decreases for lower plate velocities. It is also observed that at low velocities of the plate more time is needed for the planarization process.

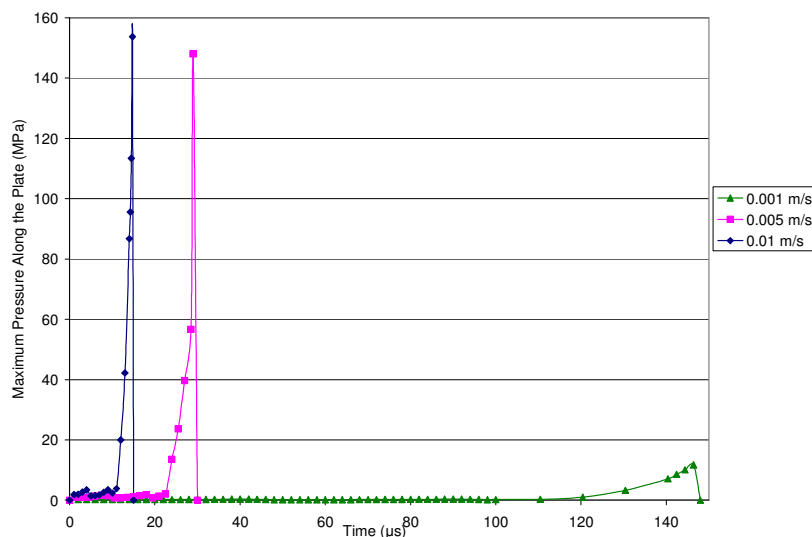


Figure 4.9 Maximum Pressure on the Plate at a Given Time for Different Plate Velocities and a Viscosity of 22 Pa·s

Figure 4.10 shows the plot for the maximum pressure exerted on the plate for different velocities of the plate. It is observed that reducing the plate velocity by ten times reduces the pressure by almost ten times. There is no significant change in the pressure when the velocity was changed from 0.01 m/s to 0.005 m/s. Newton's law of viscosity states that the force per unit area of the fluid ($\frac{F}{A}$) is proportional to the viscosity (μ) and the velocity gradient ($\frac{du}{dy}$), which is given by the following equation

[38]:

$$\frac{F}{A} = \mu \frac{du}{dy} \quad 4.2$$

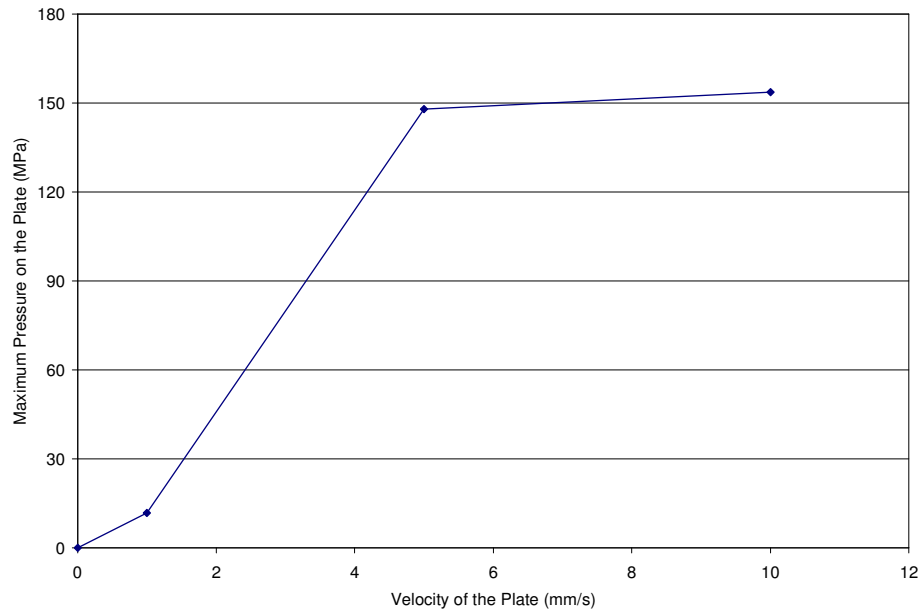


Figure 4.10 Maximum Pressure on the Plate at Different Velocities of the Plate

Since S1818 is Newtonian until a certain solvent percentage and then non-Newtonian below that solvent percentage, the force equation for power law fluids should also be considered [38]:

$$\frac{F}{A} = K \left(\frac{du}{dy} \right)^n \quad 4.3$$

where K is the flow consistency index (Pa·s). For non-Newtonian fluids, the flow consistency index is related to the viscosity by the following equation.

$$\mu = K \left(\frac{du}{dy} \right)^{n-1} \quad 4.4$$

The force acting per unit area of fluid is proportional to the velocity gradient and to the viscosity. So, as the velocity increases, the velocity gradient also increases, increasing the force acting per unit area on the fluid. This results in a higher pressure on the plate for high velocities than at low velocities.

Similar dynamic mesh simulations were carried out for different viscosities at a constant plate velocity of 0.01 m/s. A plot for the maximum pressure at different simulation times was prepared for different viscosities (Figure 4.11).

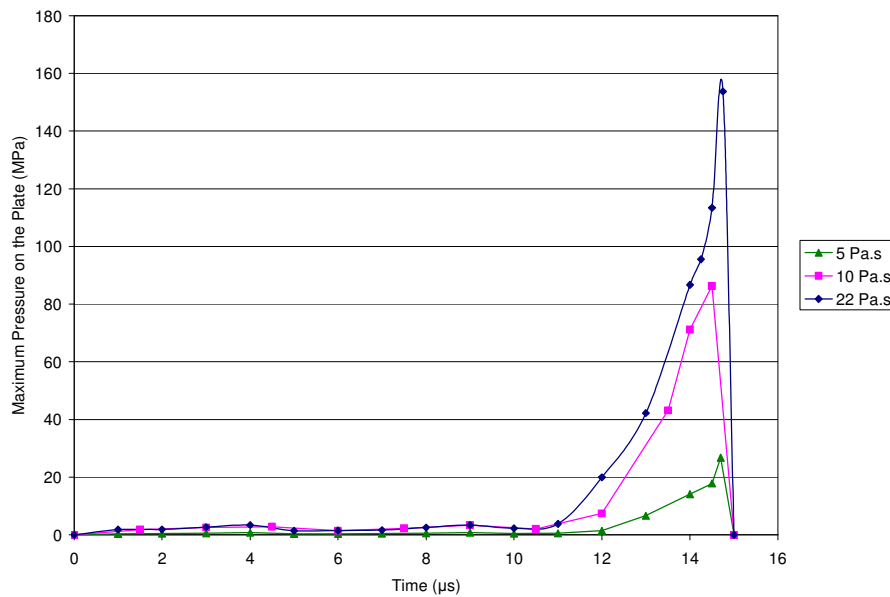


Figure 4.11 Maximum Pressure on the Plate at a Given Time for Different Viscosities and a Plate Velocity of 0.01 m/s

A maximum pressure of 150 MPa was observed for a viscosity of 22 Pa·s and decreases with decreasing viscosity. This is in agreement with the fact that the force per unit area of the fluid increases with increasing viscosity (Equations 4.1, 4.2, and 4.3). The significant increase in pressure occurs at a much later time for decreasing viscosities. The maximum pressure for different viscosities is shown in Figure 4.12. It can be inferred that reducing the viscosity from 22 Pa·s to approximately 5 Pa·s reduces the pressure on the plate by six times. It can also be observed that the maximum pressure varies increases steadily with the fluid viscosity.

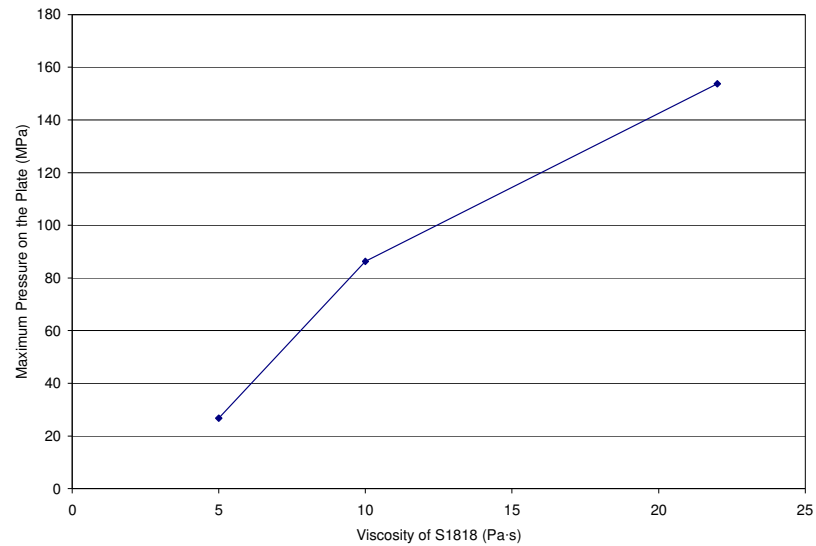


Figure 4.12 Maximum Pressure on the Plate at Different Viscosities at a Plate Velocity of 0.01 m/s

5. CONCLUSIONS AND FUTURE WORK

5.1. CONCLUSIONS

It was deduced from this work that the maximum pressure acting on the plate increases with increasing plate velocity for a given viscosity, since the velocity gradient increases with increasing velocity, resulting in an increase in pressure. The maximum pressure exerted on the plate by the fluid decreases with decreasing viscosity since fluids with higher viscosity have a higher resistance to flow. Reducing the plate velocity from 0.01 m/s to 0.001 m/s reduces the maximum pressure by approximately ten times and reducing the viscosity from 22 Pa·s to 5 Pa·s linearly reduces the maximum pressure by approximately six times. However, the pressure does not vary linearly with the plate velocity. From 0.01 m/s to 0.005 m/s, the pressure on the plate does not show any significant variation and from 0.005 m/s to 0.001 m/s, the pressure decreases by approximately 13 times.

The minimum pressure was observed for a combination of a plate velocity of 0.001 m/s and a viscosity of 5 Pa·s. The contact planarization process cannot be done at this viscosity because the fluid was observed to be tacky and would stick to the optically flat surface. Based on the range of velocities and viscosities used in this work, the optimum combination would be a plate velocity of 0.001 m/s and a viscosity between 10 and 22 Pa·s where the fluid is not tacky.

5.2. FUTURE WORK

It was not feasible to measure the viscosities for solvent percentages lower than 11.2% due to limitations of the Brookfield cone and plate viscometer. Another instrument, such as a vibration type viscometer [39], can be used to measure the viscosity for such low solvent percentages to get a more accurate viscosity-solvent percentage relation. Viscosity measurements were not carried out for solvent percentages between 21.9 and 11.2 due to lack of time. However, viscosity measurements for solvent percentages between 21.9 and 11.2 would provide the approximate solvent percentage at which non-Newtonian behavior starts. A UDF should be written to include the effect of solvent percentage on viscosity and the transition from Newtonian to non-Newtonian

behavior by using the DEFINE_PROPERTY macro as described in the FLUENT manual [18]. Unfortunately, due to the non-availability of data regarding the solvent percentage at which the fluid becomes non-Newtonian, the UDF for viscosity change and power law index is not included in this work.

In the evaporation process, the solvent present on the surface evaporates first, thus creating a mass fraction gradient in the photoresist layer. This gradient facilitates the diffusion of solvent from the bottom zones to the surface. When the UDF for the viscosity change is included in the simulation, the viscosity will vary throughout the photoresist layer. The generation of the wavy pattern might be affected by this change in viscosity gradient. The humps in wavy pattern may be pulled down slightly because of surface tension effects. However, if evaporation is much slower than the solvent diffusion through the layer, the solvent mass fraction would be almost uniform and there would not be a significant viscosity gradient. When there is no significant viscosity gradient, the change in the wavy pattern also may not be significant.

The geometry of the computational domain for the plate motion had a small gap between the mold wall and the interface to facilitate the sliding motion of the plate to the bottom of the mold (Figure 3.8). The rise of the liquid level in this gap can be avoided by modifying the geometry. This can be done by defining the edges both as a wall and as an interface as shown in Figure 5.1.

In this work, the evaporation and plate motion processes were simulated separately. The wavy pattern generated from the evaporation process simulation was not used for the planarization simulation. An uneven surface was artificially patched for the latter work. The actual process can be depicted by including both the evaporation and plate motion steps in a single simulation. The simulation done in this way would use the actual wavy pattern produced by the evaporation process in the planarization process and the pressure data obtained would be more accurate to the real situation. Since the process of transferring the volume fraction values to build the same surface would be very time consuming, it has not been included in the current work.

The plate motion simulations were performed for a fluid with different viscosities (22, 10, and 5 Pa·s) by changing the value of viscosity in the material properties panel of FLUENT. A modification in the UDF should be made to terminate the evaporation

process after a certain amount of solvent has evaporated. The fluid viscosity will be calculated based on the solvent percentage when the UDF for viscosity change is included, as described above. When the fluid viscosity reaches the required value, the planarization simulation can be started.

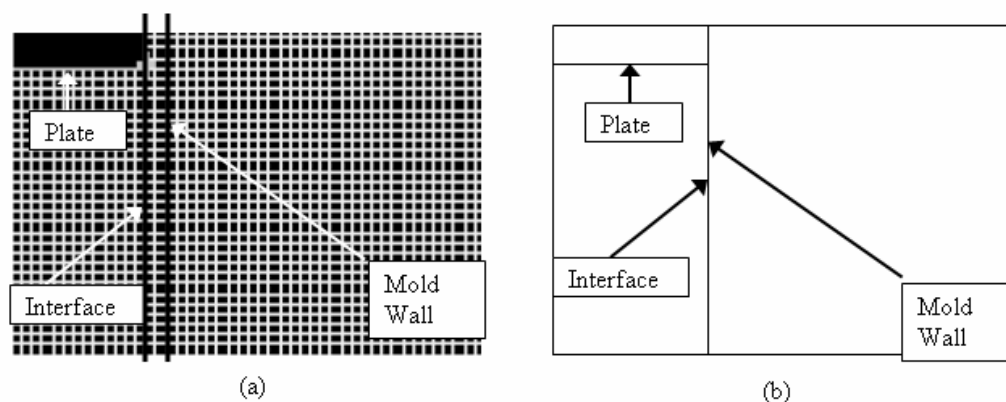


Figure 5.1 Wall and Interface Locations, (a) Current Geometry, (b) Future Modified Geometry

Simulations for plate motion were done for different velocities at a constant viscosity of 22 Pa·s and for different viscosities at a constant velocity of 0.01 m/s. The lowest velocity considered in this work was 0.001 m/s and the lowest viscosity was 5 Pa·s. Since the pressure is expected to decrease with decreasing velocity and decreasing viscosity, simulations with much lower velocities and lower viscosities can be done to decrease the pressure even further. It is to be noted that the aim is not to investigate an optimal point at which the pressure on the plate can be minimized to a global minimum. It attempts to only find a viscosity and velocity value at which the pressure on the plate is not sufficient to deform it and the fluid is not tacky. The velocity value or the viscosity value itself may be constrained by other process parameters, such as the actual apparatus limitations, limitations of the photoresist material in use, or of the mechanism lowering the plate onto the photoresist layer. In this case, simulations of the contact planarization process, with these constraints built in, will help us find out workable values for viscosity

and velocity that allows us to satisfy both the above conditions. Along with these simulations, a molecular dynamics based simulation would be more helpful than a continuum approach in studying low pressure systems such as this one.

APPENDIX A.

GOVERNING EQUATIONS OF CFD

NAVIER-STOKES EQUATIONS [19]: Set of equations to be solved for viscous flow.

Continuity equation:

Non-conservative form:

$$\frac{D\rho}{Dt} + \rho(\nabla \cdot V) = 0 \quad \text{A.1}$$

Conservative form:

$$\frac{\partial \rho}{\partial t} + \nabla \cdot (\rho V) = 0 \quad \text{A.2}$$

ρ is the density and V is the velocity vector

Momentum equations:

Non-conservative form:

$$\text{x-component: } \rho \frac{\partial u}{\partial t} = -\frac{\partial p}{\partial x} + \frac{\partial \tau_{xx}}{\partial x} + \frac{\partial \tau_{yx}}{\partial y} + \frac{\partial \tau_{zx}}{\partial z} + \rho f_x \quad \text{A.3}$$

$$\text{y-component: } \rho \frac{Dv}{Dt} = -\frac{\partial p}{\partial y} + \frac{\partial \tau_{xy}}{\partial x} + \frac{\partial \tau_{yy}}{\partial y} + \frac{\partial \tau_{zy}}{\partial z} + \rho f_y \quad \text{A.4}$$

$$\text{z-component : } \rho \frac{\partial w}{\partial t} = -\frac{\partial p}{\partial z} + \frac{\partial \tau_{xz}}{\partial x} + \frac{\partial \tau_{yz}}{\partial y} + \frac{\partial \tau_{zz}}{\partial z} + \rho f_z \quad \text{A.5}$$

where u, v , and w are the velocity components in the x, y, and z directions, p is the pressure, τ_{ij} is the shear stress exerted on a plane perpendicular to i^{th} axis in the j direction, and f_i is the body force acting in i^{th} direction.

Conservative form:

$$\text{x-component: } \frac{\partial(\rho u)}{\partial t} + \nabla \cdot (\rho u V) = -\frac{\partial p}{\partial x} + \frac{\partial \tau_{xx}}{\partial x} + \frac{\partial \tau_{yx}}{\partial y} + \frac{\partial \tau_{zx}}{\partial z} + \rho f_x \quad \text{A.6}$$

$$\text{y-component: } \frac{\partial(\rho v)}{\partial t} + \nabla \cdot (\rho v V) = -\frac{\partial p}{\partial y} + \frac{\partial \tau_{xy}}{\partial x} + \frac{\partial \tau_{yy}}{\partial y} + \frac{\partial \tau_{zy}}{\partial z} + \rho f_y \quad \text{A.7}$$

$$\text{z-component: } \frac{\partial(\rho w)}{\partial t} + \nabla \cdot (\rho w V) = -\frac{\partial p}{\partial z} + \frac{\partial \tau_{xz}}{\partial x} + \frac{\partial \tau_{yz}}{\partial y} + \frac{\partial \tau_{zz}}{\partial z} + \rho f_z \quad \text{A.8}$$

Energy equation:

Non-conservative form:

$$\rho \frac{D(e + \frac{V^2}{2})}{Dt} = \rho q + \frac{\partial(k \frac{\partial T}{\partial x})}{\partial x} + \frac{\partial(k \frac{\partial T}{\partial y})}{\partial y} + \frac{\partial(k \frac{\partial T}{\partial z})}{\partial z} - \frac{\partial(up)}{\partial x} - \frac{\partial(vp)}{\partial y} - \frac{\partial(wp)}{\partial z} + \frac{\partial(u\tau_{xx})}{\partial x} + \frac{\partial(u\tau_{yx})}{\partial y} + \frac{\partial(u\tau_{zx})}{\partial z} + \frac{\partial(v\tau_{xy})}{\partial x} + \frac{\partial(v\tau_{yy})}{\partial y} + \frac{\partial(v\tau_{zy})}{\partial z} + \frac{\partial(w\tau_{xz})}{\partial x} + \frac{\partial(w\tau_{yz})}{\partial y} + \frac{\partial(w\tau_{zz})}{\partial z} + \rho fV$$

A.9

where e is the internal energy per unit mass and T is the temperature.

Conservative form:

$$\frac{\partial}{\partial t} [p(e + \frac{V^2}{2})] + \nabla \cdot [p(e + \frac{V^2}{2})] = \rho q + \frac{\partial(k \frac{\partial T}{\partial x})}{\partial x} + \frac{\partial(k \frac{\partial T}{\partial y})}{\partial y} + \frac{\partial(k \frac{\partial T}{\partial z})}{\partial z} - \frac{\partial(up)}{\partial x} - \frac{\partial(vp)}{\partial y} - \frac{\partial(wp)}{\partial z} + \frac{\partial(u\tau_{xx})}{\partial x} + \frac{\partial(u\tau_{yx})}{\partial y} + \frac{\partial(u\tau_{zx})}{\partial z} + \frac{\partial(v\tau_{xy})}{\partial x} + \frac{\partial(v\tau_{yy})}{\partial y} + \frac{\partial(v\tau_{zy})}{\partial z} + \frac{\partial(w\tau_{xz})}{\partial x} + \frac{\partial(w\tau_{yz})}{\partial y} + \frac{\partial(w\tau_{zz})}{\partial z} + \rho f \cdot V$$

A.10

EULER EQUATIONS [19]: Set of equations to be solved for inviscid flow.**Continuity equation:**

Non-conservative form:

$$\frac{D\rho}{Dt} + \rho \nabla \cdot V = 0$$

A.11

Conservative form:

$$\frac{\partial \rho}{\partial t} + \nabla \cdot (\rho V) = 0$$

A.12

Momentum equations:

Non-conservative form:

$$\text{x-component : } \rho \frac{Du}{Dt} = -\frac{\partial p}{\partial x} + \rho f_x$$

A.13

$$\text{y-component: } \rho \frac{Dv}{Dt} = -\frac{\partial p}{\partial y} + \rho f_y$$

A.14

$$\text{z-component: } \rho \frac{Dw}{Dt} = -\frac{\partial p}{\partial z} + \rho f_z \quad \text{A.15}$$

Conservative form:

$$\text{x-component: } \frac{\partial(\rho u)}{\partial t} + \nabla \cdot (\rho u V) = -\frac{\partial p}{\partial x} + \rho f_x \quad \text{A.16}$$

$$\text{y-component: } \frac{\partial(\rho v)}{\partial t} + \nabla \cdot (\rho v V) = -\frac{\partial p}{\partial y} + \rho f_y \quad \text{A.17}$$

$$\text{z-component: } \frac{\partial(\rho w)}{\partial t} + \nabla \cdot (\rho w V) = -\frac{\partial p}{\partial z} + \rho f_z \quad \text{A.18}$$

Energy equation:

Non-conservative form:

$$\rho \frac{D}{Dt} \left(e + \frac{V^2}{2} \right) = \rho q - \frac{\partial(up)}{\partial x} - \frac{\partial(vp)}{\partial y} - \frac{\partial(wp)}{\partial z} + \rho f \cdot V \quad \text{A.19}$$

Conservative form:

$$\frac{\partial}{\partial t} \left[p \left(e + \frac{V^2}{2} \right) \right] + \nabla \cdot \left[p \left(e + \frac{V^2}{2} \right) V \right] = \rho q - \frac{\partial(up)}{\partial x} - \frac{\partial(vp)}{\partial y} - \frac{\partial(wp)}{\partial z} + \rho f \cdot V \quad \text{A.20}$$

The shear stresses are related to the viscosity μ by the following relations.

$$\tau_{xx} = 2\mu \left[\frac{\partial u}{\partial x} - \frac{1}{3}(\nabla \cdot V) \right] \quad \text{A.21}$$

$$\tau_{yy} = 2\mu \left[\frac{\partial v}{\partial y} - \frac{1}{3}(\nabla \cdot V) \right] \quad \text{A.22}$$

$$\tau_{zz} = 2\mu \left[\frac{\partial w}{\partial z} - \frac{1}{3}(\nabla \cdot V) \right] \quad \text{A.23}$$

$$\tau_{xy} = \tau_{yx} = \mu \left[\frac{\partial u}{\partial y} + \frac{\partial v}{\partial x} \right] \quad \text{A.24}$$

$$\tau_{yz} = \tau_{zy} = \mu \left[\frac{\partial w}{\partial y} + \frac{\partial v}{\partial z} \right] \quad \text{A.25}$$

$$\tau_{zx} = \tau_{xz} = \mu \left[\frac{\partial u}{\partial z} + \frac{\partial w}{\partial x} \right]$$

A.26

APPENDIX B.

UDF FOR EVAPORATION AND CONTACT PLANARIZATION

UDF for evaporation:

```
# include "udf.h"
# define domain_ID 2

/*DEFINE_ADJUST is used to calculate the value of volume fraction in each cell. The parameter
adjust_gradient is the UDF name and the parameter domain is the pointer to the domain to which this
UDF is applied. This function is executed at every iteration. [18]*/

DEFINE_ADJUST(adjust_gradient, domain)
{
    Thread *t;
    cell_t c;
    face_t f;

/*The domain pointer FLUENT passes is the mixture level domain. As multiphase flow is being used,
the phase level domain pointer has to be used. Get_Domain is used to get the phase level domain
pointer. [18]*/

    domain = Get_Domain(domain_ID);

/*Looping over the cells to store the value of volume fraction as a user defined scalar.*/

    thread_loop_c(t, domain)
    {
        begin_c_loop(c, t)
        {
            C_UDSI(c, t, 0) = C_VOF(c, t);
        }
        end_c_loop(c, t)
    }
}

/*DEFINE_MASS_TRANSFER is used to specify a mass transfer coefficient based on the volume
fraction gradient. The parameters passed are: liq_gas_source – name of the UDF, cell – index of the
cell to which the UDF is being applied, thread – pointer to the mixture level thread, from_index – ID of
the phase from which mass is being transferred, from_species_index – ID of the species which is being
```

*transferred, to_index – ID of the phase to which mass is being transferred, and to_species_index – ID of the species to which mass is transferred. [18] */*

```
DEFINE_MASS_TRANSFER(liq_gas_source, cell, thread, from_index, from_species_index, to_index, to_species_index)
```

```
{
    real m_lg, vof_grad;
    real T_SAT = 373.15;
    Thread *gas = THREAD_SUB_THREAD(thread, from_index);
    Thread *liq = THREAD_SUB_THREAD(thread, to_index);

    m_lg = 0.0;
```

*/*Calculating the volume fraction gradient based on the user defined scalar and storing it in a memory variable.*/*

```
vof_grad = NV_MAG(C_UDSI_G(cell, thread, 0));
C_UDMI(cell, thread, 0) = vof_grad ;
```

*/*Specifying the volume fraction gradient condition for mass transfer. The cutoff gradient is chosen in a trial and error method to obtain the proper shape of the interface.*/*

```
if (fabs(vof_grad) >4.5e5)
{
    m_lg =10;
}

return (m_lg);
}
```

UDF for plate motion:

```
#include "udf.h"
#define velocity -0.01
```

*/*plate_bottom_ID and the vacuum_phase_ID are obtained from FLUENT*/*

```
#define plate_bottom_ID 10
#define vacuum_phase_ID 0
int stop =0;
```

/*DEFINE_CG_MOTION is used to define the plate motion by specifying the velocity components. The parameters passed are: moving_wall – name of the UDF, t – thread of the cell to which the UDF is applicable, vel – linear velocity, omega – angular velocity, time – flow time, and dttime – time step size. [18]*/

```
DEFINE_CG_MOTION(moving_wall,t,vel,omega,time,dttime)
{
    Message("\n STOP = %d, \n ", stop);
    if(stop == 0)
    {
        vel[0]= 0;
        vel[1]= -0.01;
        vel[2]= 0;
        omega[0]= 0;
        omega[1]= 0;
        omega[2]= 0;
    }
    else
    {
        vel[0] = 0;
        vel[1] = 0;
        vel[2] = 0;
        omega[0] = 0;
        omega[1] = 0;
        omega[2] = 0;
    }
}
```

/*DEFINE_ADJUST is used to calculate the volume being displaced by the plate motion and the amount air needed to be removed. The mass and momentum source terms are calculated accordingly.*/

```
DEFINE_ADJUST(plate_motion,d)
{
    Domain *domain = Get_Domain(1);
```

```

Thread *mt = Lookup_Thread(domain, plate_bottom_ID), *t0;
Thread **allt;
cell_t c0;
face_t f;
real total_mass_sink, mass_sink, mom_sink[ND_ND], dvol,
airvol, flow_time, time_step, sum;
allt = THREAD_SUB_THREADS(mt);
real area_v[ND_ND], area;

if(first_iteration)
{
    flow_time = CURRENT_TIME;
    time_step = CURRENT_TIMESTEP;
    sum = 0.0;

/*Looping over all the faces in the domain to calculate the volume displaced by the plate, volume of the
air being removed, and the source terms*/

begin_f_loop(f, mt)
{
    c0 = F_C0(f, allt[vacuum_phase_ID]);
    t0 = F_C0_THREAD(f, allt[vacuum_phase_ID]);
    F_AREA(area_v, f, mt);
    area = NV_MAG(area_v);
    dvol = area*fabs(velocity)*time_step;
    airvol = C_VOLUME(c0, t0)*C_VOF(c0, t0);

    sum += C_VOF(c0, t0);
    if(C_VOLUME(c0, t0)/2 < dvol)
    {
        dvol = C_VOLUME(c0, t0)/2.0;
    }

    if( airvol < dvol)
        mass_sink = -airvol*C_R(c0, t0)/(time_step*C_VOLUME(c0, t0));
    else
        mass_sink = -dvol*C_R(c0, t0)/(time_step*C_VOLUME(c0, t0));
    mom_sink[0] = mass_sink*0.0;
}

```



```
mom_sink[1] = mass_sink*velocity;
```

/*Allocating the memory variables to the source terms*/

```
C_UDMI(c0,t0,0) = flow_time;
C_UDMI(c0,t0,1) = mass_sink;
C_UDMI(c0,t0,2) = mom_sink[0];
C_UDMI(c0,t0,3) = mom_sink[1];
}
end_f_loop(f,mt);
```

/*Specifying the condition for stopping the plate.*/

```
if(fabs(sum)< 0.001)
    stop = 1;
}
}
```

/*DEFINE_SOURCE is used to return the mass source value to FLUENT*/

```
DEFINE_SOURCE(air_mass, c, t, ds, eqn)
{
    real flow_time;
    flow_time = CURRENT_TIME;
    if ((flow_time == C_UDMI(c,t,0)) && (stop == 0))
        return C_UDMI(c,t,1);
    else
        return 0.0;
}
```

/*DEFINE_SOURCE is used to return the x-momentum source value to FLUENT*/

```
DEFINE_SOURCE(x_mom, c, t, ds, eqn)
{
    real flow_time;
    flow_time = CURRENT_TIME;
    if ((flow_time == C_UDMI(c,t,0)) && (stop == 0))
```

```
        return C_UDMI(c,t,2);
    else
        return 0.0;
}
```

/*DEFINE_SOURCE is used to return the y-momentum source value to FLUENT*/

```
DEFINE_SOURCE(y_mom, c, t, ds, eqn)
{
    real flow_time;
    flow_time = CURRENT_TIME;
    if ((flow_time == C_UDMI(c,t,0)) && (stop == 0))
        return C_UDMI(c,t,3);
    else
        return 0.0;
}
```

REFERENCES

- [1] Franssila, S. (2004) "Introduction to Microfabrication," John Wiley and Sons, New York
- [2] "SKW1-1 150mm Wafer Specifications," (2001), SKW Associates Inc., Santa Clara, CA (www.testwafer.com/PDF/skw1-1_150_spec.pdf)
- [3] MICRON "www.micron.com/applications," accessed 06/15/07
- [4] Shapiro, C. (1974) "The Lithographers Manual," Graphic Arts Technical Foundation, Pittsburgh, 5th Ed.
- [5] Zant, P.V. (2000) "Microchip Fabrication," McGraw-Hill, New York
- [6] Dobkin, D.M. and Zuraw, M.K. (2003) "Principles of Chemical Vapor Deposition," Springer, New York
- [7] Jaeger, R.C. (2001) "Introduction to Microelectronic Fabrication," Prentice Hall, New Jersey
- [8] Klein, L.C. (1994) "Sol-Gel Optics: Processing and Applications," Springer, New York
- [9] Wolf, S. (2002) "Silicon Processing for the VLSI Era: Volume 4 – Deep-Submicron Process Technology," Lattice Press, Sunset Beach, CA
- [10] Shih, W. and Daffron M.G. (2003) "A Novel Planarization Process for Providing Global Planarity for IC Manufacturing," Proc. Int. Symp. Microelectronics, 813-818
- [11] Chiu, G.L.T. and Shaw, J.M. (1997) "Optical Lithography: Introduction," IBM J Res Dev, 41(1,2):3-6
- [12] Brewer Science Inc., Rolla, MO, "www.brewerscience.com/products/con-tact/the-con-tactR-process," accessed 06/15/07
- [13] Fuller, G.E. (2000) "Handbook of Semiconductor Manufacturing Technology," Marcel Dekker, Inc., New York
- [14] Ying, L. (2004) "Slurry Chemistry Effects on Copper Chemical Mechanical Planarization," Masters Thesis, University of Central Florida, Orlando
- [15] Prybyla, J.A. "Device Fabrication Involving Surface Planarization," Patent Number-6,048,799, Apr 11, 2000
- [16] CON-TACT Team (2004) "CON-TACT® Planarization, a Novel Method to Achieve Global and Local Planarization," ARC Symposium, Leuven, Belgium
- [17] Shaw, C.T. (1992) "Using Computational Fluid Dynamics," Prentice Hall, New Jersey
- [18] Richardson, L.F. (1910) "The Approximate Arithmetical Solution by Finite Differences of Physical Problems Including Differential Equations, with an Application to the Stresses in a Masonry Dam," Philos T R Soc A, 210:307-357

- [17] FLUENT[®] “www.fluent.com/about/cfdhistory.htm,” accessed 06/16/07
- [19] Anderson, J.D. (1995) “Computational Fluid Dynamics: The Basics with Applications,” McGraw-Hill, New York
- [20] Chung, T.J. (2002) “Computational Fluid Dynamics,” Cambridge University Press, New York
- [21] LeVeque, R.J. (2002) “Finite Volume Method for Hyperbolic Problems,” Cambridge University Press, New York
- [22] Reddy, J.N. (1993) “An Introduction to the Finite Element Method,” McGraw-Hill, New York
- [23] Wesseling, P. (2001) “Principles of Computational Fluid Dynamics,” Springer, New York
- [24] Kreyszig, E. (2001) “Advanced Engineering Mathematics,” John Wiley & Sons, Inc., New York
- [25] Patnakar, S. (1980) “Numerical Heat Transfer and Fluid Flow,” Hemisphere, New York
- [26] Versteeg, H.K. and Malalasekera, W. (1995) “An Introduction to Computational Fluid Dynamics: The Finite Volume Method,” Longman Scientific & Technical, New York
- [27] Garbero, M., Vanni, M., and Fritsching, U. (2006) “Gas/Surface Heat Transfer in Spray Deposition Processes,” *Int J Heat Fluid Fl*, 27:105-122
- [18] FLUENT 6.2 Documentation, FLUENT, Inc.
- [28] Lytle, L.W.H. and Hileman, B. (1996) “Application of CFD Tool in Designing a Fountain Plating Cell for Uniform Bump Plating of Semiconductor Wafers,” *IEEE T Compon Pack B*, 19(1):131-137
- [29] Deen, W.M. (1998) “Analysis of Transport Phenomena,” Oxford University Press, New York
- [30] FLUENT Newsletter (1997) “Boeing uses FLUENT to Cut Costs,” 6(2):12 (<http://www.fluent.com/about/news/newsletters/97v6i2/a8.htm>)
- [31] FLUENT Application Brief (2001) “Tank Sloshing Validation,” Example 161 (<http://www.fluent.com/solutions/aerospace/pdfs/ex161.pdf>)
- [19] Pantula, S.R. “Numerical Simulation of Water Splash when Driving through Water,” Master Thesis, Chalmers Institute of Technology, Gothenburg, Sweden
- [20] Andersson, V. (2003) “Simulation of Two Phase Flows in a Distributor Application,” Master Thesis, Lund Institute of Technology, Lund, Sweden
- [21] Kokturk, T. (2005) “Design and Performance Analysis of a Reversible Axial Flow Fan,” Master Thesis, Middle East Technical University, Turkey
- [22] Mayer, D.T., Dittmer, C., and Faigle, W. (1997) “Printing Inks and Related Subjects,” (http://www.hdm-stuttgart.de/projekte/printing-inks/b_selec0.htm, accessed 07/11/07)

- [37] “More Solutions to Sticky Problems - A Guide to Getting More From Your Brookfield Viscometer,” (1998) Brookfield Engineering Labs, Inc.
- [38] McCabe, W.L., Smith, J.C., and Harriott, P. (2003) “Unit Operations of Chemical Engineering,” McGraw Hill, New York
- [39] Tai, H., Seki, J., Kida, T., and Kobayashi, T. (2004) “Vibration-Type Viscometer using a Triangular Bimorph Transducer – Measurement of High Viscosity by Low Frequency Operation,” *Jpn J Appl Phys*, 43(5B):3088-3089

VITA

Shanti Vusirikala was born on April 9, 1984 to Latha and Mrutyunjaya Rao Vusirikala at Vizianagaram, India. She completed her Bachelor of Technology in Chemical Engineering from Jawaharlal Nehru Technological University in April 2005. She joined University of Missouri-Rolla in Fall 2005 for a Master of Science program in Chemical Engineering and received the degree in December 2007.

